STATE-SPACE MODELING OF A PLANAR SOLID OXIDE FUEL CELL

by

Gülsün Demirezen

B.S., Industrial Engineering, Yeditepe University, 2013

Submitted to the Institute for Graduate Studies in

Science and Engineering in partial fulfillment of

the requirements for the degree of

Master of Science

Graduate Program in Systems and Control Engineering

Boğaziçi University

2016

STATE-SPACE MODELING OF A PLANAR SOLID OXIDE FUEL CELL

APPROVED BY:

Assist. Prof. Oktay Demircan	…..……..…….....
(Thesis Co-Supervisor)	
Prof. Dr. Yağmur Denizhan	…….
(Thesis Co-Supervisor)	
Prof. Dr. Ahmet Kerim Avcı	……..
Assoc. Prof. Selmiye Alkan Gürsel	……...

DATE OF APPROVAL: 2/09/2016

ACKNOWLEDGEMENTS

I would like to thank all the people who contributed in some way to the work described in this thesis. Firstly, I thank my academic advisor and thesis supervisor, Prof. Dr. Yağmur Denizhan, for the useful comments, remarks and engagement through the learning process of this master thesis and my education in Boğaziçi University. During this thesis, she contributed to a rewarding graduate school experience by giving me intellectual freedom in my work, supporting my attendance at various conferences and engaging me in new ideas. I am also thankful for the excellent example she has provided as a successful woman engineer and professor. I have gained a life-term lessons from her.

Furthermore, I would like to thank to my co-supervisor Assist. Prof. Oktay Demircan for introducing me to the topic as well for the support on the way and for many insightful conversations during the development of the ideas in this thesis, and for helpful comments on the text. I appreciate his patience on teaching me the subject from the beginning. I am thankful to Assist. Prof. Oktay Demircan for putting so much time and effort on me. In developing the ideas presented here, I have received helpful input from Fuel Cells and Energy Laboratory at Boğaziçi University, under the supervision of Assist. Prof. Oktay Demircan. I would like to express my deepest gratitude to Prof. Dr. Ahmet Kerim Avcı and Assoc. Prof. Selmiye Alkan Gürsel for being in my thesis committee.

I gratefully acknowledge the financial support by Turkish Research Council (TUBITAK) under grand number of 214Z094. I also would like to extend my appreciation to members of Fuel Cells and Energy Laboratory in Department of Chemistry at Boğaziçi University; Aktan Polat, Ayşenur Eslem Kısa, Benazir Fazlıoğlu and Furkan Işık for their essential contributions. It has always been joyful to work with my colleagues. I also thank to Duygu Tuncel and Kübra Eren for their comments on this work.

Last but not least, I wish to thank my parents, Ömer and Kıymet Demirezen and my sister Günseli Demirezen; my gratitude to them is beyond words and I always feel their support and love. Also, I thank to my aunt, Zülfiye Kaçar for the moral support since the beginning of my education life. I also thank to my grandfathers; for all they were, and all they had done for me. I am thankful to my grandmothers, Mahinur Demirezen and Nazife

Kaçar for teaching me how to put effort and patience on a subject. I would like to thank my loved ones and dear friends, who have supported me throughout entire process, both by keeping me harmonious and helping me putting pieces together.

ABSTRACT

STATE-SPACE MODELING OF A PLANAR SOLID OXIDE FUEL CELL

In this thesis, state-space modeling approach is applied to a complete planar Solid Oxide Fuel Cell (SOFC) system. Several simulations of the dynamic system have been performed for 400°C to 800°C as operating temperature. In addition, the results of the simulations are compared with experimental results obtained at Fuel Cells and Energy Laboratory at Boğaziçi University. The validity of the model is checked through these comparisons.

In this study, the performance of a planar SOFC system is investigated on basis of simulations obtained on a MATLAB® software platform by using dynamic modeling approach.

This study allows us to observe influence of various material parameters on the operation of the planar SOFC and to determine the limiting factors of mechanism considered. In addition, the model supports the interpretation of the experimental results obtained at Fuel Cells and Energy Laboratory at Boğaziçi University.

ÖZET

DÜZLEMSEL KATI OKSİT YAKIT HÜCRESİNİN DURUM-UZAY MODELLEMESİ

Bu tezde, durum-uzay modellemesi yaklaşımı kullanılarak, bütün bir düzlemsel katı yakıt hücresi sistemi, devimsel olarak modellenmiştir. Devimsel sistemin benzetimleri 400^0C ile 800^0C arasında, bilgisayar ortamında gerçekleştirilmiştir. Ek olarak, benzetim sonuçları ile Yakıt Hücreleri ve Enerji Laboratuvarı'nda gerçekleştirilen deneysel sonuçlar karşılaştırılmıştır. Modelin geçerliliği, deneysel sonuçlar ile yapılan karşılaştırılmalar ile denetlenmiştir.

Bu çalışmada, düzlemsel katı yakıt hücresinin verimi, bir bilgisayar yazılımı olan MATLAB® üzerinden yapılan, devimsel modelleme yöntemi kullanılarak gerçekleştirilen benzetimler ile incelenmiştir.

Bu çalışma, düzlemsel katı yakıt hücresini çalıştırırken, kullanılan malzemelerin özelliklerinin ve kısıtlayıcı etmenlerin hücreye olan etkisini gözlemlemeyi mümkün kılar. Ek olarak, bu modelleme çalışması, Boğaziçi Üniversitesi'nde bulunan Yakıt Hücreleri ve Enerji Laboratuvarı'nda konu ile ilişkili deney sonuçlarının yorumlanmasına yardımcı olur.

TABLE OF CONTENTS

ACKNOWLEDGEMENTS iii

ABSTRACT v

STATE-SPACE MODELING OF A PLANAR SOLID OXIDE FUEL CELL v

ÖZET vi

LIST OF FIGURES vii

LIST OF TABLES ix

LIST OF ACRONYMS / ABBREVIATIONS x

1. INTRODUCTION 1

1.1. Energy Sources 1

1.2. Fuel Cells 1

1.2.1. Solid Oxide Fuel Cells 3

1.2.2. Polarization in SOFCs 5

1.2.3. Electrochemical Impedance Spectroscopy (EIS) 6

1.3. Solid Oxide Fuel Cell Principles 10

1.3.1. Voltage Output 11

1.3.2. Current Output 14

2. A SIMPLIFIED MODEL FOR THE PLANAR SOFC 15

2.1. Scope of Modeling 15

2.2. Dynamic Modeling of Planar SOFC 16

2.2.1. Dynamic Modeling Approach 17

2.2.2. Diffusion 18

2.2.3. Diffusion Coefficient 23

2.2.4. Voltage 24

2.2.5. Equivalent Circuit 26

2.2.6. Model in the State-Space Form 28

3. RESULTS and DISCUSSION 33

3.1. Model Parameters 33

3.2. Comparison of Simulated Planar SOFC Performance Test Results with Empirical Performance Test Results 37

3.3. Simulated Planar SOFC Performance Test Results with different H_2 operating Parameters 45

4. CONCLUSION 48

5. FUTURE WORK 50

6. REFERENCES 51

LIST OF FIGURES

Figure 1.1. Fuel cell types. 2

Figure 1.2. SOFC configurations. 4

Figure 1.3. Typical fuel cell polarization curve. 6

Figure 1.4. Sinusoidal voltage and current at a given frequency: $1/T_P$. 7

Figure 1.5. Schematic representation of EIS Nyquist plot. 9

Figure 2.1. Equivalent circuit of inherent impedance. 26

Figure 2.2. Equivalent circuit of a single SOFC. 27

Figure 3.1. Schematic representation of a planar SOFC fabricated at Fuel Cells and Energy Laboratory in Boğaziçi University. 33

Figure 3.2. Comparison of fabricated and operated planar SOFC at Fuel Cells and Energy Laboratory and modeled planar SOFC in terms of voltage, current density and power density at 400°C. 38

Figure 3.3. Comparison of fabricated and operated planar SOFC at Fuel Cells and Energy Laboratory and modeled planar SOFC in terms of voltage, current density and power density at 450°C. 39

Figure 3.4. Comparison of fabricated and operated planar SOFC at Fuel Cells and Energy Laboratory and modeled planar SOFC in terms of voltage, current density and power density at 500°C. 40

Figure 3.5. Comparison of fabricated and operated planar SOFC at Fuel Cells and Energy Laboratory and modeled planar SOFC in terms of voltage, current density and power density at 550°C. 41

Figure 3.6. Comparison of fabricated and operated planar SOFC at Fuel Cells and Energy Laboratory and modeled planar SOFC in terms of voltage, current density and power density at 600°C. 42

Figure 3.7. Comparison of fabricated and operated planar SOFC at Fuel Cells and Energy Laboratory and modeled planar SOFC in terms of voltage, current density and power density at 650°C. 43

Figure 3.8. Comparison of fabricated and operated planar SOFC at Fuel Cells and Energy Laboratory and modeled planar SOFC in terms of voltage, current density and power density at 700°C. 43

Figure 3.9. Comparison of fabricated and operated planar SOFC at Fuel Cells and Energy Laboratory and modeled planar SOFC in terms of voltage, current density and power density at 800°C. 44

Figure 3.10. Comparison of simulated planar SOFC at different partial pressures of H_2 in terms of voltage, current density and power density at 400°C. 46

Figure 3.11. Simulated planar SOFC at different partial pressure of H_2 as 0.54 in terms of voltage and current density at the temperature ranges between 400°C to 800°C with an increment of at 50°C. 47

Figure 3.12. Simulated planar SOFC at different partial pressure of H_2 as 0.27 in terms of voltage and current density at the temperature ranges between 400°C to 800°C with an increment of at 50°C. 47

LIST OF TABLES

Table 2.1. Input and Output Variables of the Modelled Planar SOFC. 19

Table 3.1. Parameters used in simulation..... 37

Table 3.2. Diffusional volume parameters. 38

Table 3.3. Partial pressure values used in simulation. 38

Table 3.4. Ohmic resistance, R_o (Ω) values of YSZ at different temperatures and hydrogen partial pressures..... 39

Table 3.5. Charge transfer resistance, R_{ct} (Ω) values of YSZ at different temperatures and hydrogen partial pressures. 39

Table 3.6. Charge transfer capacitance, C (Farad) values of YSZ at different temperatures and hydrogen partial pressures. 40

Table 3.7. Area Specific Resistance, ASR (Ω) values of YSZ at different temperatures and hydrogen partial pressures. 40

LIST OF ACRONYMS / ABBREVIATIONS

ASR	Area-specific resistance
AV	Alternative voltage
CHP-units	Combined heat and power-units
EIS	Electrochemical Impedance Spectroscopy
LSM	Lanthanum strontium manganite
LSV	Linear sweep voltammetry
Ni/YSZ	Nickel/zirconia cermet
OCV	Open Current Voltage
PEM	Polymer Electrolyte Membrane
SOFC	Solide Oxide Fuel Cell
tpb	Triple phase boundary
TW	Terawatts
V-I-P	Voltage-current-power
YSZ	Yttria-stabilized zirconi

1. INTRODUCTION

1.1. Energy Sources

Renewable and non-renewable energy can be considered as two main categories of energy sources. Renewable energy is energy generated from natural energy sources. They often provide energy in the following areas [1]:

- Electricity generation,
- Air and water heating/cooling,
- Transportation.

In the energy literature there exists various terminologies referring almost to the same notion with slight difference in emphasis. The terms “renewable” and “alternative” are used almost to designate the same category of energy sources other than fossil fuels.

Non-renewable energy sources such as petroleum, coal and natural gas emit greenhouse gases to the atmosphere causing global warming. Because of industrialization and increase in world population, the demand in energy supply has drastically increased. The worldwide energy demand is assumed to be approximately 12 terawatts (TW) by 2050 [2]. On the other hand, there is a considerable decrease in non-renewable energy sources. Therefore, renewable energy sector must be open to new developments and technologies.

1.2. Fuel Cells

Fuel cells, because of their broad range of applications and its potential as a mobile, sustainable energy source constitute an important domain of investigation [3]. As an electrochemical device, in a fuel cell, hydrogen and oxygen are combined to produce electricity, while water and heat are the by-products. Among other methods of power generation, fuel cells confer various important environmental superiorities due to their low

emissions of sulphur and nitrogen oxides and hydrocarbon pollutants in addition to reduced CO_2 emissions.

During the past decade, on account of the developments in material science and manufacturing engineering, researchers have put significant efforts on fuel cells due to their environmental advantages and high efficiencies.

Although fuel cells have gained popularity within the last decades their history is actually longer. In 1839, William Grove demonstrated the concepts of fuel cells by suggesting some novel constructions for the first electric cells [4]. The term ‘fuel cell’ was first used by Mond and Longer to describe their device having with a porous platinum electrode. As shown in Figure 1.1, a fuel cell consists of two electrodes (anode and cathode) separated by an electrolyte.

Compared to other types of energy conversion technologies such as gas turbines and reciprocating engines, fuel cells offer more efficient use of fuels. Different types of fuel cells are categorized according to the nature of the electrolyte they employ.

The electrolyte dictates the most suitable operating temperature range of a fuel cell. Various types of fuel cells consist of direct methanol fuel cell, PEM (Polymer Electrolyte Membrane) fuel cell, alkaline fuel cell, phosphoric acid fuel cell, molten carbonate fuel cell and SOFC (Solid Oxide Fuel Cell). The operating principle is similar for all types of fuels cells.

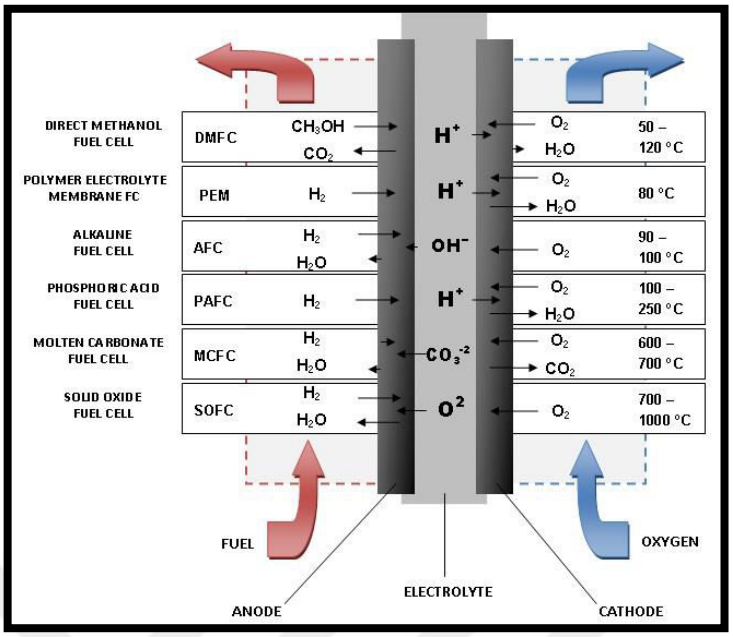


Figure 1.1. Fuel cell types.

Fuel cell applications can be categorized according to efficiency and environmental considerations. For instance, in urban areas local pollution is an issue related with the environmental consideration of fuel cells. On the other hand, utilization of fuels are related with the efficiency considerations. The range of applications is not limited to large-scale distributed power plants, but also micro-scale applications are being developed due to their higher power densities and longer lifetimes.

Broadly, the use of fuel cells can be classified into three areas as [5]:

- Power for transportation,
- Stationary power generation,
- Portable power generation.

1.2.1. Solid Oxide Fuel Cells

In 1899 Walther H. Nernst discovered that yttria-stabilized zirconia (YSZ) is a solid-state oxygen ion conductor at high temperatures. Walter Schottky, one of the Nernst's students, proposed the idea of SOFC, which came to fruition when Emil Baur and Hans Preis built the first functioning SOFC in 1937 [7].

The name of the solid ceramic material at the center of the device is the solid oxide fuel cell. SOFC's are considered as high temperature fuel cells which use dense YSZ. It is noted that here oxygen, O^{2-} combines with hydrogen H^{+} to generate water and heat. SOFC produce electricity at a high operating temperature of 1000°C, SOFC produce electricity. There are some advantages of SOFC. First of all, they operate a rather at high efficiency of 50–60%. Secondly, a separate reformer is not required to extract hydrogen from the fuel because the fuel cell has an internal reforming capability [8].

Unlike most other types of fuel cells, SOFCs may be constructed at various different. According to these geometries, SOFC types can be classified as planar cell, tubular, monolithic and coplanar. The SOFC configurations can be seen in Figure 1.2.

The fabrication process of a planar SOFC is similar to that of other single cells. At Fuel Cells and Alternative Energy Laboratory in Boğaziçi University, yttria-stabilized zirconia (YSZ) for the electrolyte, lanthanum strontium manganite (LSM) for the cathode and nickel/zirconia cermet (Ni/YSZ) for the anode are used to fabricate a planar SOFC. Self-supporting and externally supported cells are the two types of planar SOFC. The structural support of the cell, namely the thickest layer, characterizes the type of the design of the single cell. These designs are electrolyte-supported, anode-supported, or cathode-supported single cells. On the other hand, in the externally supported configuration, the single cell is configured as a porous substrate or thin layers on interconnect [7].

The advantages of SOFC can be listed as follows [9]:

- Compared to other fuel cell types, SOFCs have higher electrical efficiency.
- Because of their high operating temperature, the CO produced by SOFCs is converted to CO_2. This means that SOFCs have relatively low exhaust emission.
- H_2 or hydrocarbon fuels are used to operate the cell. Also, SOFCs do not need expensive noble metals such as platinum.
- As SOFCs operate at high temperature, the heat gained after operating SOFCs is considerable. The efficient utilization of the heat gained are supplied via CHP-units (combined heat and power-units). Therefore, the overall energy efficiency is also observed.

In Figure 1.2, the anode, electrolyte, and cathode are designated with black, light gray, and dark gray colors, respectively. The (a) planar and are anode, electrolyte, and cathode supported from top to bottom; (b) tubular configuration; (c) coplanar configuration; (d) monolithic configuration shown with interconnects.

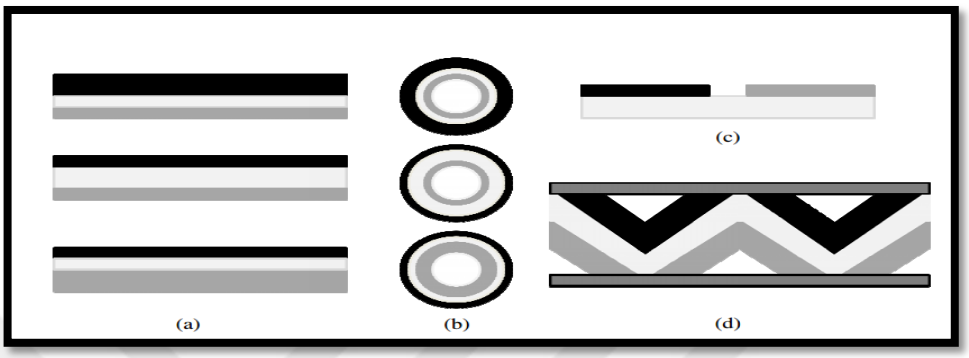


Figure 1.2. SOFC configurations [8].

1.2.2. Polarization in SOFCs

In a SOFC system, the circuit is a closed circuit. SOFC is connected to a load to operate. The production of the current is caused due to electrochemical reactions. However, the potential of the cell is decreased. Because, internal nonreversible voltage losses are investigated. These losses depend on the current and can be categorized as three main mechanisms [10]:

- Ohmic resistance losses: As the ions follow, in the solid electrolyte phases ohmic resistance losses are observed. Meanwhile, electrons also flow. This also causes ohmic resistance losses. In other words, ohmic resistance losses are investigated by the electrical resistances of the electrodes and resistance of ion transport in the electrolyte. The area-specific resistance, ASR is based on 1cm² of the cell. In order to reduce the polarization caused by ohmic resistance losses, there are three conventional methods. Firstly, thin electrolyte is designed. Secondly, electrodes are fabricated from materials that have high conductivity properties. Lastly, interconnect materials are considered according to these two design spectra.
- Concentration overpotentials: Triple phase boundary, tpb, is a term used to define the active reaction zone. Occurred reactions are electrochemical reactions. Through

porous electrodes, charge carrying reactants reduce Nernst potential at this zone. As electrochemical reactions are directly dependent on the concentration of the reactants and oxidants, these overpotentials are named as concentration overpotentials.

- Activation overpotentials: In order for electrochemical reactions to start, there is an activation energy is needed. These reactions are considered as forward reactions. At the anode, the fuel is oxidized. At the cathode, reduction of the oxygen is happened. In order to calculate the potential of the operating cell, the summation of these losses are subtracted from the reversible potential.

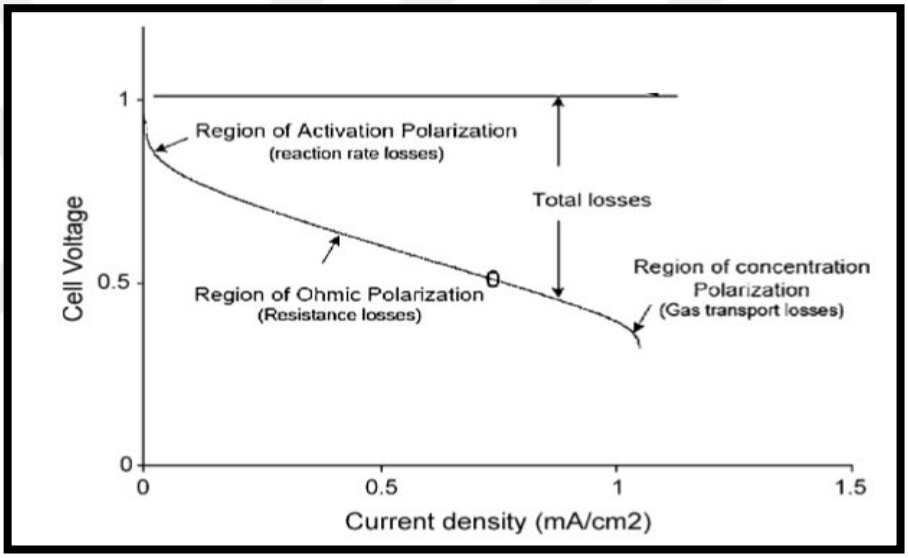


Figure 1.3. Typical fuel cell polarization curve (modified from [11]).

1.2.3. Electrochemical Impedance Spectroscopy (EIS)

Chemical and physical processes of electrochemical systems are investigated via Electrochemical Impedance Spectroscopy (EIS). The alternative current, AC flows and is monitored through the system as the alternative voltage, AV is applied.

To measure the opposition to current flow, resistance is used. Namely, resistance is the capability of a circuit element to resist the flow of electrical current. Resistance is measured in ohms, symbolized by the Greek letter omega (Ω). Georg Simon Ohm (1784-

1854) gave the name of this unit of resistance. Ohm investigated the dependency of voltage and current by considering the resistance. Ohm's law is stated in Equation 1.1 as follows:

$$R = V / I \tag{1.1}$$

In Equation 1.1, R is the resistance, V is the voltage and I is the current of a circuit. Due to the fact that the real life applications of circuit elements show much more complex behaviour, impedance is used to simply this complexity. Because, impedance is a similar to resistance in terms of measuring the capability of a circuit to resist the flow of electrical current. With regard to independence of frequency and in phase of voltage and current, the impedance is not limited by the simplification of the ideal resistance [12].

In order to measure the electrochemical impedance of a fuel cell, alternating (sinusoidal) voltage at various frequencies is applied to it. In circuits, where the resistance to the flow of electrical current depends on the dynamic changes in the current, the motion of resistance has to be replaced by its more general complex counterpart impedance, which is still measured in Ohms but is a complex quantity, $\underline{Z}$.

Figure 1.4 shows the sinusoidal voltage with a frequency, $f = 1/\mathrm{T_P}$ applied to a linear device and the current measured as a measured as a response to it. The ratio of the amplitudes of the voltage and current correspond to the magnitude of the impedance $\underline{Z}$ this specific frequency, while the phase difference between the sinusoidal voltage and current gives the phase of $\underline{Z}$ at the same frequency.

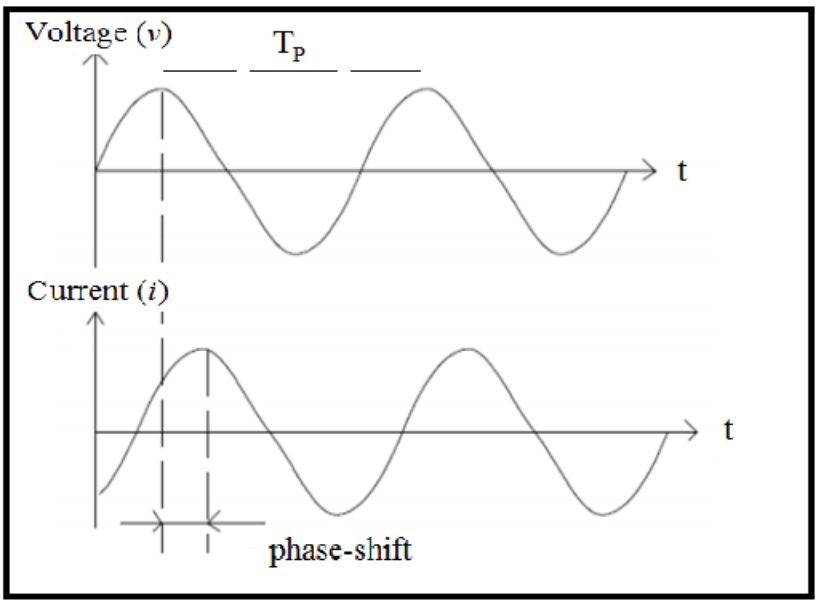


Figure 1.4. Sinusoidal voltage and current at a given frequency: $1/T_P$.

The signal response can be shown as a function of time as follows:

$$v(t) = v_o \cos(\omega t) \tag{1.2}$$

In Equation 1.2, $v(t)$ is the potential at time t, ω is angular frequency and v_o is the amplitude of the signal. Equation 1.3 shows the relationship between frequency, $f\,(\mathrm{Hz}) = \frac{1}{T_P}$ where T_P (sec) is the period and ω (rad/sec) is angular frequency, is as follows:

$$\omega = 2\pi f = \frac{2\pi}{T_P} \tag{1.3}$$

In order to characterize the behaviour of the SOFC system, we will consider the applied voltage, v (t) (potential difference) as the input and the resulting current flow as the response, i(t). At a given angular frequency, ω the equation for i(t) is as follows:

$$i(t) = i_o \cos(\omega t - \phi) \tag{1.4}$$

The Ohm's Law can be extended to sinusoidal voltage and current using Euler's relationship which expresses sinusoidal functions in terms of complex exponential functions represented from Equation 1.5 to Equation 1.9 are as follows:

$$e^{j\alpha} = \cos\alpha + j\sin\alpha \tag{1.5}$$

$$v(t) = v_o \,.\, \mathrm{re}\{e^{j\omega t}\} \tag{1.6}$$

$$i(t) = i_o \,.\, \mathrm{re}\{e^{j(\omega t - \phi)}\} \tag{1.7}$$

$$Z_o \cos\phi + j\, Z_o \sin\phi = Z_{\mathrm{re}}(\omega) + j\, Z_{\mathrm{im}} \tag{1.8}$$

$$\underline{Z}(\omega) = \frac{v_o \mathrm{e}^{\,j\omega t}}{i_o \mathrm{e}^{\,j(\omega t - \phi)}} = \frac{v_o}{i_o}\mathrm{e}^{\,j\phi} \tag{1.9}$$

In Equation 1.9, ϕ is the phase of $\underline{Z}$ at ω, and $Z_o = \frac{v_o}{i_o}$ is the magnitude of $\underline{Z}$ at ω. In the equations above, j is used to represent $\sqrt{-1}$. As it can be seen in Equation 1.9, $\underline{Z}(\omega)$ is comprised by two parts. These parts are real and imaginary parts that are Z_{re} and Z_{im}, respectively. In order to obtain a "Nyquist plot", the real part is plotted on the x-axis and the imaginary part is plotted on the y-axis for angular frequencies ω varying from 0 to ∞.

In Figure 1.5, R_s represents the bulk resistance. Left hand side of the curve represents high frequency part on the Nyquist plot. R_s is controlled by interconnects of the cell and electrolyte part of the cell. R_{ct} is the polarization resistance. R_{ct} can also be represented as $R_{polarization}$. All the electrochemical processes related to the electrodes are displayed by $R_{polarization}$. Processes that contribute to the impedance of electrode reactions are associated with the number of impedance arcs in the plot.

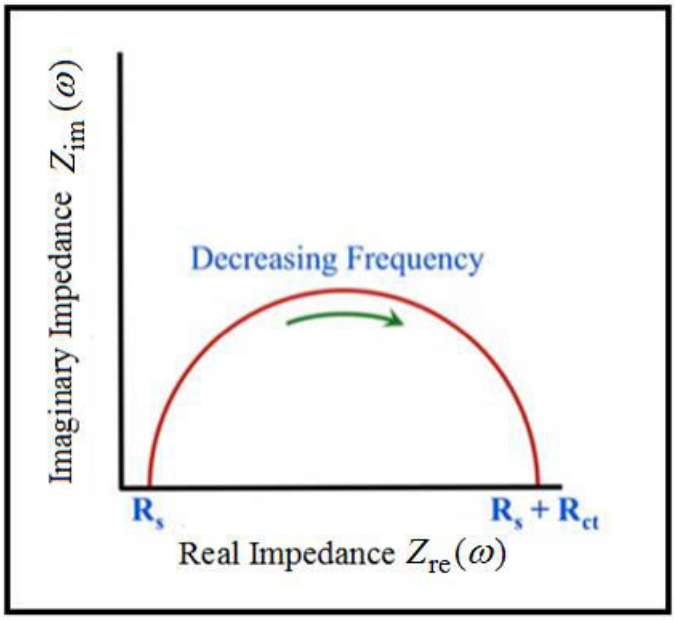


Figure 1.5. Schematic representation of EIS Nyquist plot.

The real part, Z_{re}, on the x-axis represents resistive processes of impedance curve. The imaginary part, Z_{im}, on the y-axis shows capacitive processes of an impedance curve.

Plot format of a Nyquist plot enables to observe the effects of the ohmic resistance easily. Due to the same reason, the data taken at sufficiently high frequencies, extrapolating the semicircle toward the left is easy. Therefore, down to the x-axis, the ohmic resistance can be read. When the ohmic resistance changes, the shape of the curve does not change. As a result, the results of two separate experiments, which differ only in the position of the reference electrode can be investigated.

1.3. Solid Oxide Fuel Cell Principles

Through electrochemical reactions, fuel's chemical energy is converted into electrical energy by an SOFC system. In this study, hydrogen, H_2 is utilized as the fuel and oxygen is used as the oxidant in electrochemical reactions. Oxygen, O_2 is supplied from the air. By-products of the electrochemical reaction are heat, water, and electricity is

produced. Because a SOFC system is not limited by Carnot efficiencies, the system efficiency is higher compared to conventional combustion engines [13].

It is noted that a planar SOFC has three bonded layers. The layers are named as cathode, anode and electrolyte. The electrodes are separated by electrolyte. In this study, the reaction of the Hydrogen, H_2 with oxygen produces water. However, in case of the fuel is a hydrocarbon, then carbon dioxide, CO_2 is the product. Eventually, in all types of the fuels, the power is generated due the flow of electricity by through the migration of releasing electrons.

In an SOFC that utilize H and O_2, the electrochemical reactions that occur at anode and cathode respectively are as follows [14]:

$$H_2 + O^{2-} \rightarrow H_2O + 2e^- \quad (1.10)$$

$$½\ O_2 + 2e^- \rightarrow O^{2-} \quad (1.11)$$

Overall electrochemical reaction is shown in Equation 2.3.

$$H_2 + ½\ O_2 \rightarrow H_2O \quad (1.12)$$

1.3.1. Voltage Output

The difference between the enthalpy of a system and the product of its entropy and absolute temperature is called “Gibbs Free Energy” [15]. In the ideal situation, according to Gibbs Free Energy formula stated in Equation (1.13), electrical work is equal to Gibbs Free Energy released.

$$\Delta\bar{g}_f = 2FV_{OC} \quad (1.13)$$

$\Delta\bar{g}_f$ denotes Gibbs Free Energy, V_{OC} denotes the open circuit voltage and F is the Faraday’s constant. The electrical work done in moving charge through the SOFC is equal

to the work done per unit charge on one mole of electrons. In order for a cell to complete the work, the moving charge should follow the entire circuit [16]. In this study, planar SOFC considered also has a reversible open circuit voltage.

F, Faraday constant is 96.485 C mol^{-1}. The "2" in the equation represents the number of electrons that flow for one mole of hydrogen oxidized. For an ideal system, the electrical work during the reaction is equal to the Molar Gibbs free energy released, $\Delta\bar{g}_f$ [17].

The performance indices of a SOFC is measured in terms of V_{OC}, the ideal open circuit voltage which depends on the temperature of the reactions involved. A variety of fuel-specific parameters are directly related to V_{OC}. V_{OC} of a planar SOFC varies with the partial pressure of the fuel supplied. In this thesis, we take H_2 as the fuel of the cell.

Molar Gibbs free energy depends on the partial pressure of the fuel in addition to pressure of the reactant. In addition, Nernst equation investigates the relation of the reaction temperature onto the Molar Gibbs free energy. This dependence can be expressed as [18]:

$$V_{OC} = V^{o} + \frac{RT}{n\mathrm{F}} \ln\left(\frac{\text{reactant activity}}{\text{product activity}}\right) \tag{1.14}$$

V^{o} is the maximum Open Current Voltage generated under standard conditions (1 atmospheric pressure), n is number of electrons transferred in the reaction, T is the temperature of the electrode surface in K. R is the Universal Gas Constant, 8.314 J/mol.

Reactant and product activities are dependent on the molar concentration of reactants/products. The Nernst equation for the SOFC fabricated at Fuel Cells and Energy Sources Laboratory at Boğaziçi University, can be written as [19]:

$$V_{OC} = V^{o} + \frac{RT}{2\mathrm{F}} \ln\left(\frac{(a-H_2)(b-O_2)}{c-H_2O}\right) \tag{1.15}$$

In this study, H_2 is the fuel. Since two electrons are transferred in the reaction $n = 2$ in Equation 1.14. In Equation 1.15, "a", “b”, and “c” are the activities of the specific reactant or product and are expressed in molarity of a solution. Molarity is considered as the measure of strength of a solution. Activity can be expressed as:

$$p = \frac{\text{Partial Pressure}}{\text{Standart Pressure}} = \frac{p}{p^o} \tag{1.16}$$

Overall, the activities of H_2, O_2 and H_2O can be written as follows respectively:

$$a_{H_2} = \frac{p_{H_2}}{p^o}, a_{O_2} = \frac{p_{O_2}}{p^o}, a_{H_2O} = \frac{p_{H_2O}}{p^o{}_{H_2O}} \tag{1.17}$$

Here, p_{H_2}, p_{O_2} and p_{H_2O} are reactant partial pressures, p^o is the standard pressure, $p^o{}_{H_2O}$ is the vapour pressure of the steam at the temperature concerned. V_{OC} is called Nernst voltage. In this study, it is assumed that gases behave as ideal gases. Therefore, standard pressure is equal to the vapour pressure of the steam at the concerned temperature. Accordingly, Equation 1.17 can be simplified as:

$$V_{OC} = V^o + \frac{RT}{2F} \ln\left(\frac{(pH_2)(pO_2)^{1/2}}{(pH_2O)}\right) \tag{1.18}$$

Irreversibility reduces the cells voltage. They are mainly activation loss, ohmic loss and concentration loss. The irreversible voltage, V_{IR} is usually modeled in the steady state form as follows [20]:

$$V_{IR} = V_{OC} - i_{out} R_{in} - A\ln\left(\frac{i_{out}}{i_o}\right) - B\ln\left(1 - \frac{i_{out}}{i_l}\right) \tag{1.19}$$

In Equation 1.19, i_{out} is the current produced by the planar SOFC, R_{in} is the inherent resistance of the cell, i_o is the exchange current of the cell, and i_l is the limiting current. Limiting current at which the fuel is used up at a rate equal to its maximum supply rate. Exchange current of the cell is a significant parameter. Because, exchange current is the parameter of weighting activity of catalyst reaction. *A* and *B* are coefficients for activation

loss and concentration loss, respectively. The losses of potential are ohmic loss, activation loss, and concentration loss and shown as Equation 1.20, 1.21, and 1.22 respectively.

$$\text{Ohmic loss} = i_{out} R_{in} \tag{1.20}$$

$$\text{Activation loss} = A \ln\left(\frac{i_{out}}{i_o}\right) \tag{1.21}$$

$$\text{Concentration loss} = B \ln\left(1 - \frac{i_{out}}{i_l}\right) \tag{1.22}$$

1.3.2. Current Output

In this study, the transit dynamics of the reactions are neglected. Therefore, the relationship between reactions and current can be identified as follows [20]:

$$i_{out} = 2\mathrm{F}J^r_{H_2} = 2\mathrm{F}J^r_{H_2O} = 4\mathrm{F}J^r_{O_2} \tag{1.23}$$

Here, J^r is the reaction rate at reaction sites in μmol/s. For H_2, superscript *r* is the fuel consumption rate at tpb. For H_2O, superscript *r* represents water vapour production rate at tpb.

Efficiency of SOFC is directly related to the current output. However, maximum current that a planar SOFC can output is limited by various factors. These factors are [21]:

- Reactant supply rates,
- Reaction rates and the area where the reactions take place,
- Dependencies on voltage and load impedance,
- Ionic conductivity of electrolyte.

2. A SIMPLIFIED MODEL FOR THE PLANAR SOFC

2.1. Scope of Modeling

This modeling study consists dynamic modeling as linear sweep voltammetry, LSV. In this thesis, in order to investigate the operation of a planar SOFC, dynamic modeling study is conducted by simulating the model with different operating parameters such as temperature and partial pressure of the fuel, H_2. In this part of the study, state-of-art SOFC models and EIS parameter identification for SOFC in the open literature are reviewed. In addition, the scope of this thesis work is given.

Mathematical models are beneficial for progress of numerous power generation technologies. Because, they are probably more significant for fuel cell development. It is often difficult to characterize the internal operation of a fuel cell. There are various reasons that cause difficulties on investigation what is happening inside of the fuel cell. These reasons are ionic conduction, simultaneous heat transfer and coupled electrochemical reactions. Therefore, multidisciplinary approaches are required to conduct a comprehensive study of SOFC. Through modeling studies, it is relatively easier to understand the internal characteristics of SOFC [22]. Investigations on chemistry and the internal physics of fuel cells are often difficult. Because both chemical and physical processes in the fuel cells are complex. Also, it is limited to accessing inside of the fuel cells [23]. In addition, fuel cells simulation is a helpful approach to focus experimental researches. In order to improve the quality of experimental researches, simulation is used to investigate the accuracy of experimental parameters. Furthermore, designing and optimizing SOFC systems, mathematical models are considered as one of the most significant approaches. Specifically, testing the operational factors of SOFCs, dynamic models are investigated. Namely, developed dynamic models are considered to check whether characteristics of specific type of fuel cell can meet the requirements of an application [24]. Also, cost-effectiveness of a specific design can be studied through dynamic modeling approaches. Because of its importance, in the past 2 decades there has been tremendous progress on computational approaches for SOFCs. Hence,

interdisciplinary papers have been published. After representing the modeling work, the results of the simulations are also reported [25-29].

Triple phase boundaries, tpb are the boundaries where fuel and oxidant, electrolyte and anode or cathode meet. In a typical operation of a planar SOFC, H_2 is fed in the cell. Afterwards, H_2 follows through the layers to tpb. There layers are the gas boundary layers and porous support layers. After the layers, H_2 reaches to porous electrodes. Eventually, at tpb, the reactions occur. As the fuel, H_2 is transported through the parts of the planar SOFC. These processes are called "mass transport" dynamics.

In the light of these explanations, mass transport processes are one of the remarkable dynamic sources of planar SOFCs, operated under uniform temperature condition.

At Fuel Cells and Alternative Energy Laboratory at Boğaziçi University, the researches on developing high quality materials for various temperature SOFCs have been continued. Measurements on performance of the planar SOFC are held via LSV. Briefly, the performance of a planar SOFC system is investigated on basis of simulations conducted on a MATLAB® software platform by using dynamic modeling approach.

In this thesis, the mathematical model is applied in a complete fuel cell system model. Several simulations of the dynamic system have been performed for 400^{o}C to 800 ^{o}C as operating temperature. In addition, the results of the simulations are compared with experimental results conducted at Fuel Cells and Energy Sources Laboratory at Boğaziçi University. The validity of the model is checked through these comparisons.

2.2. Dynamic Modeling of Planar SOFC

Macro-dynamic modeling is necessary to conduct studies on investigating dynamic characteristics of SOFC due to micro-dynamic models are not suitable for macro-applications as on the papers of Yamamura et al. [30] and Perumar et al. [31]. The first macro-dynamic modeling of SOFC belongs to Achenbach [32]. This work analyzes the

transient cell voltage performance of a cross-flow planar SOFC due to the temperature changes and the perturbations in current density. However, this model does not examine the species dynamics on stack-level. Padullés et al. [33] has mentioned in species dynamics on his study. Sedghisigarchi et al. [34] has adopted the work of Achenbach and Padullés et al. by considering both species dynamics and heat transfer dynamics. These works do not consider the processes of species transport from flow bulk to triple phase boundary (tpb). In addition to considering only lumped dynamic behavior of species along fuel/air channel, Qi et al. [35] proposed a model that lies between macro-scale and micro-scale. This work of Qi et al. enables not only to examine the cell-level but also to consider stack-level model. Because, the basis of this modeling approach proposes that the cell-level model is a building block for a stack-level model.

2.2.1. Dynamic Modeling Approach

In this part of the modeling, the aim is to demonstrate dynamic behaviors of output voltage and output current of a planar SOFC. The assumptions made in dynamic modeling are as follows:

- Gas diffusion difficulties and parameters are neglected.
- Temperature is uniform throughout the elemental volume.
- Partial pressures of gasses in flow bulks surrounding the elemental volume are uniform.

In order to examine the external characteristics, input variables are derived from the operating inputs of the planar SOFC produced by researchers at Fuel Cells and Energy Sources Laboratory in Boğaziçi University. In addition, one of the key factors to investigate the external characteristics of a planar SOFC is to define the factor that affects the reaction rates and reactant supplies. Partial pressures of reactants in gas bulks have a direct impact on reaction rates and reactant supplies.

The fuel, which happens to be hydrogen in this study, and the oxygen supply constitute the inputs given to the cell in the experimentation. Since partial pressures of the reactants

in the gas bulks are directly determined by these physical inputs, partial pressures have been taken as the input variables in our model.

It should be noted that the output current is directly affected by the area specific resistance value, R_{AS}, which needs to be included as a parameter in the dynamic model. The value of R_{AS}, can be obtained either empirically or EIS simulation results. Area specific resistance value is often expressed as ASR, shortly. In this thesis, empirical values of R_{AS} has been used as the parameter value in the dynamic model.

Table 2.1. Input and Output Variables of the Modelled Planar SOFC.

Inputs	
$p_{H_2}^b$	Partial pressure of hydrogen in anode gas bulk
$p_{O_2}^b$	Partial pressure of oxygen in cathode gas bulk
$p_{H_2O}^b$	Partial pressure of water vapour in anode gas bulk
Outputs	
v_{out}	Voltage output of planar SOFC
i_{out}	Current output of planar SOFC

2.2.2. Diffusion

Campanari et al. [41], mentioned on their paper that the path of mass transport from the flow bulk to the reaction site. At first, mass transportation happens from the flow bulk to the cell surface layer. Secondly, transportation is observed through the electrode that is porous to reaction sites. It means that, in the first stage, the diffusion of the mass flux

happens through the boundary layer to the cell surface. In the second stage, inside the porous electrode, mass flux diffusion happens inside the porous electrode. Therefore, in order to develop a mass transport function in the model, it is a must to consider Fick's Diffusion Law where flux density, j_{fd} is considered as a dependent variable. Because flux is directly proportional to the steepness of the gradient. The Fick's Law is given in Equation 2.1 as follows:

$$j_{\mathrm{fd}} = -D\frac{\mathrm{dC_m}}{\mathrm{dx}} \tag{2.1}$$

where D is a coefficient based on the particular substance being measured. $\frac{\mathrm{dC}}{\mathrm{dx}}$ is steepness of the gradient. C_m is the mass concentration. According to Fick's Law, mass transport equation can be written as:

$$\frac{\delta C_{\mathrm{m}}}{\delta t} = D\frac{\partial^2 A}{\partial x^2} \tag{2.2}$$

where D is the diffusion coefficient and x is the diffusion depth.

Although there are studies conducted on calculating the concentration values at tpb by finite element method as stated in literature, in this thesis study Laplace transform is used to define the analytical dynamic relations. Because, special variables are not involved in Laplace transform and this is an advantage of using Laplace transform. In this thesis, the equations of the transform is derived from Qi et. al [35] and the book of Wayland [42].

In Equation 2.2, if the Laplace transform is performed, the partial differential equation to the ordinary differential equation is converted [43]:

$$\frac{\mathrm{d}^2 C_{\mathrm{m}}(s)}{\mathrm{d}x^2} - \frac{s}{D}C_{\mathrm{m}}(s) = 0 \tag{2.3}$$

where the boundary conditions are

$$j^{\mathrm{r}}(s) = -D\frac{\mathrm{d}C_{\mathrm{m}}(s)}{\mathrm{d}x}|_{x=0},\ C^{\mathrm{b}}(s) = C_{\mathrm{m}}(s)|_{x=L} \tag{2.4}$$

The solution of Equation 2.3 is as follows:

$$C(s)(x)=\frac{C^{\mathrm{b}}(s)+\frac{j^{\mathrm{r}}(s)}{\sqrt{Ds}}}{\exp\left(\sqrt{\frac{s}{D}}L\right)+\exp\left(-\sqrt{\frac{s}{D}}L\right)}\exp\left(\sqrt{\frac{s}{D}}L\right)+ \\ \frac{C^{\mathrm{b}}(s)-\frac{j^{\mathrm{r}}(s)}{\sqrt{Ds}}\exp\left(\sqrt{\frac{s}{D}}L\right)}{\exp\left(\sqrt{\frac{s}{D}}L\right)+\exp\left(-\sqrt{\frac{s}{D}}L\right)}\exp\left(-\sqrt{\frac{s}{D}}L\right) \tag{2.5}$$

At tpb, the diffusion depth, x is zero. A is the flow area. If the gases are assumed to be ideal, the partial pressure in the vicinity of tpb, p^{tpb} is shown as follows [44]:

$$p^{\mathrm{tpb}}(s)=-\frac{\exp\left(\sqrt{\frac{s}{D}}L\right)-\exp\left(-\sqrt{\frac{s}{D}}L\right)}{\exp\left(\sqrt{\frac{s}{D}}L\right)+\exp\left(-\sqrt{\frac{s}{D}}L\right)}\frac{1}{\sqrt{Ds}}\frac{RT}{A}J^{\mathrm{r}}(s)+ \\ \frac{2}{\exp\left(\sqrt{\frac{s}{D}}L\right)+\exp\left(-\sqrt{\frac{s}{D}}L\right)}p^{\mathrm{b}}(s) \tag{2.6}$$

After defining p^{tpb}; mass flow rate, J^{s} can be calculated.

$$J^{\mathrm{s}}=AD\left(\mathrm{d}C/\mathrm{d}x\right)|_{x=L} \tag{2.7}$$

The dynamic relation of mass flow rate is driven as follows [44]:

$$J^{s}(s)=\frac{2}{\exp\left(\sqrt{\frac{s}{D}}L\right)+\exp\left(-\sqrt{\frac{s}{D}}L\right)}J^{r}(s)+\frac{\exp\left(\sqrt{\frac{s}{D}}L\right)-\exp\left(-\sqrt{\frac{s}{D}}L\right)}{\exp\left(\sqrt{\frac{s}{D}}L\right)+\exp\left(-\sqrt{\frac{s}{D}}L\right)}\sqrt{Ds}\frac{A}{RT}p^{b}(s) \tag{2.8}$$

In order to get rid of the exponential part of Equation 2.8, Taylor's expansions can be used to hold the sufficient approximations. Taylor's expansions of $\exp\left(\sqrt{\frac{s}{D}}L\right)$ and $\exp\left(-\sqrt{\frac{s}{D}}L\right)$ are as follows:

$$\exp\left(\sqrt{\frac{s}{D}}L\right)=1+\sqrt{\frac{s}{D}}L+\frac{1}{2}\frac{s}{D}L^{2}+\frac{1}{6}\frac{s^{3/2}}{D^{3/2}}L^{3}+\frac{1}{24}\frac{s^{2}}{D^{2}}L^{4}+O\left(\sqrt{\frac{s}{D}}L\right) \tag{2.9}$$

$$\exp\left(-\sqrt{\frac{s}{D}}L\right)=1-\sqrt{\frac{s}{D}}L+\frac{1}{2}\frac{s}{D}L^{2}-\frac{1}{6}\frac{s^{3/2}}{D^{3/2}}L^{3}+\frac{1}{24}\frac{s^{2}}{D^{2}}L^{4}+O\left(\sqrt{\frac{s}{D}}L\right) \tag{2.10}$$

Afterwards, Equation 2.9 and 2.10 are substituted into Equation 2.5 and 2.6, the partial pressure in the vicinity of tpb, p^{tpb} is yield by neglecting higher order terms [44]:

$$p^{tpb}(s)=G_{Jp}J^{r}(s)+G_{pp}p^{b}(s) \tag{2.11}$$

$$J^{r}(s)=G_{JJ}J^{r}(s)+G_{pJ}p^{b}(s) \tag{2.12}$$

where

$$G_{\mathrm{Jp}} = \frac{-\frac{L}{D} - \frac{L^3}{6D^2}s}{1 + \frac{L^2}{2D}s + \frac{L^4}{24D^2}s^2} \frac{RT}{A} \tag{2.13}$$

$$G_{\mathrm{pp}} = \frac{1}{1 + \frac{L^2}{2D}s + \frac{L^4}{24D^2}s^2} \tag{2.14}$$

$$G_{\mathrm{JJ}} = \frac{1}{1 + \frac{L^2}{2D}s + \frac{L^4}{24D^2}s^2} \tag{2.15}$$

$$G_{\mathrm{pJ}} = \frac{Ls}{1 + \frac{L^2}{2D}s + \frac{L^4}{24D^2}s^2} \frac{A}{RT} \tag{2.16}$$

p^{tpb} is the partial pressure in the vicinity of tpb, p^{b} the partial pressure in gas bulks, J^{s} the gas flow into the outer surface of porous material, J^{r} the gas consumption or water production rate at tpb, L the layer thickness, A the cell area, D the effective area diffusion coefficient, R the gas constant, and T is the temperature.

After these calculations, dynamic behavior of partial pressure in the vicinity of tpb, p^{tpb} can be observed. Also, gas flows at electrode surface is identified. Because, the behaviors of gas consumption rate and bulk pressure without relying on concentration distribution along the diffusion path [44].

These dynamic identifications include solely two parameters. The first parameter is diffusion coefficient, *D*. From correlation equations of the book of Welty et al. [45], *D* can be calculated. According to fluid mechanics, flow velocity is derived. The diffusion layer, *L* depends only on flow velocity.

2.2.3. Diffusion Coefficient

Welty et al. [45] has reported on their book that, in porous materials, the effective diffusion coefficient is adjusted.

$$D_{\text{eff}} = \frac{\varepsilon}{\tau} D \tag{2.17}$$

where ε is the porosity, τ the tortuosity of porous materials, and D is the total diffusion coefficient. According to Welty et al. [45], through Knudsen diffusion, the total diffusion coefficient can be driven as follows:

$$\frac{1}{D} = \frac{1}{D_{12}} + \frac{1}{D_{\text{k}}} \tag{2.18}$$

where D_{12} is the binary diffusion coefficient, and D_{k} is the Knudsen diffusion coefficient. Welty et al. [45] claim that Knudsen diffusion can be neglected in case of pores being large enough. In this study, as the planar SOFC operated by Demircan's Research Group has large pores, Knudsen diffusion is neglected. Fuller's correlation enables to model the binary diffusion coefficient, D_{12} [46]:

$$D_{12} = \frac{1.013^{-2}\, T^{1.75} \left(\frac{1}{M_1} + \frac{1}{M_2} \right)^{0.5}}{P \left[\left(\sum_{i=1}^{2} v_i \right)_1^{1/3} + \left(\sum_{i=1}^{2} v_i \right)_2^{1/3} \right]^2} \tag{2.19}$$

where T is the temperature, M_1 and M_2 are the molar mass of gases 1 and 2, namely H_2 and O_2, $\left(\sum v_i\right)_1$ and $\left(\sum v_i\right)_2$ are the diffusional volumes of gases 1 and 2, respectively and P is the total pressure.

2.2.4. Voltage

Although the operation of the planar SOFC produced and fabricated successfully at Fuel Cells and Energy Laboratory at Boğaziçi University, it is expected to observe some losses in the cell's voltage produced. These losses are concentration loss, ohmic loss and activation loss. Obviously, the losses affect the voltage output. Namely, the dynamic behavior of the voltage is affected by the losses. As the reactions take place at tpb, The Nernst Equation in Equation 1.18, can be written more precisely as follows:

$$V_{OC} = V^o + \frac{RT}{2F} \ln\left(\frac{p_{H_2}^{tpb} \left(p_{O_2}^{tpb} \right)^{1/2}}{p_{H_2O}^{tpb}} \right) \tag{2.20}$$

where $p_{H_2}^{tpb}$, $p_{O_2}^{tpb}$ and $p_{H_2O}^{tpb}$ are the partial pressures in the vicinity of tpb. Due to the operation of the fuel cell, the fuel, H_2 is consumed. Also, O_2 is utilized. These consumptions lead to reductions in the vicinity of tpb.

Concentration loss is generally corrected by a static concentration loss term [47]. Activation losses are those losses associated with the initial dramatic voltage losses in fuel cells. These losses are basically representative of a loss of overall voltage at the expense of forcing the reaction to completion, which is forcing the hydrogen to split into electrons and protons, and then combine with the oxide ion and returning electrons. This loss is often termed over potential, and is essentially the voltage difference between the two terminals. Through experimentation, Tafel was able to describe these losses mathematically [48]. Tafel produced figures that showed direct correlation between the current density and the output voltage, at lower currents. Under the consideration of entire losses, the activation loss, which is the potential consumed to overcome the activation energy barrier, is described by the Butler-Volmer correlation [49]:

$$i_{CD} = i_o \left\{ \exp\left(\beta \frac{nF\eta_{act}}{RT} \right) - \exp\left[-(1-\beta) \frac{nF\eta_{act}}{RT} \right] \right\} \tag{2.21}$$

where i_{CD} is the electrode current density, β is the transfer coefficient and i_o the exchange current. Chan et al. [50], has reported that β is taken as 0.5 for many fuel cell applications. In this study, β is also taken 0.5. Therefore, via Equation 2.21, activation loss can be written as follows:

$$\eta_{\text{act,a}} = \frac{2RT}{nF} \sinh^{-1}\left(\frac{i}{2i_{o,\text{a}}} \right) \tag{2.22}$$

$$\eta_{\text{act,c}} = \frac{2RT}{nF} \sinh^{-1}\left(\frac{i}{2i_{o,\text{c}}} \right) \tag{2.23}$$

$\eta_{\text{act,a}}$ and $\eta_{\text{act,c}}$ are activation losses of anode and cathode, respectively.

Temperature, partial pressures and the activation energy affect the exchange currents in anode and cathode. Campanari et al. [41], calculated the exchange currents as follows:

$$i_{o,\text{a}} = \left(7\times10^9 \text{ A}\right) \times \left(p_{H_2}^{\text{tpb}} p_{H_2O}^{\text{tpb}} \right) \exp\left(-\frac{E_{\text{act,a}}}{RT} \right) \tag{2.24}$$

$$i_{o,\text{c}} = \left(7\times10^9 \text{ A}\right) \times \left(p_{O_2}^{\text{tpb}} \right)^{0.25} \exp\left(-\frac{E_{\text{act,c}}}{RT} \right) \tag{2.25}$$

where $E_{\text{act,a}}$ and $E_{\text{act,c}}$ are anode activation energy of anode and cathode, respectively. In this thesis, Equation 2.24 and 2.25 is used to compensate the activation to investigate the irreversible voltage which is calculated as follows:

$$E = E^{o} + \frac{RT}{2F}\ln\left(\frac{p_{H_2}^{tpb}\left(p_{O_2}^{tpb}\right)^{1/2}}{p_{H_2O}^{tpb}}\right) - \eta_{act,a} - \eta_{act,c} \quad (2.26)$$

2.2.5. Equivalent Circuit

Wagner et al. [50], stated that whole inherent impedance can be approximated by one RC unit as diffusion impedance is neglected. It means that, the error caused due to fluctuation in the voltage must be reduced. This changes in voltage is smoothed by double layer capacitance. Inherent impedance of SOFC has two double layer capacitance: cathode charge double layer capacitance and anode charge double layer capacitance. Also, inherent impedance consists of resistance processes namely electron reaction resistances, ohmic resistance and grain boundary resistances.

Ohmic loss is the voltage drop that is caused by the current flows through the impedance. Dynamic behavior of inherent impedance can be observed by modeling it as equivalent RC circuits and it is shown in Figure 2.1.

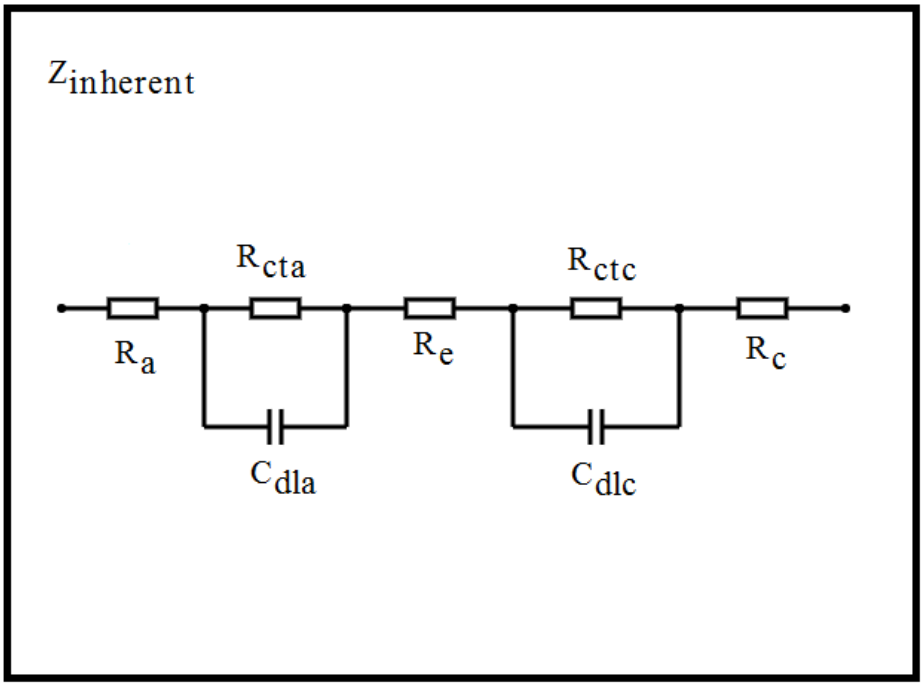


Figure 2.1. Equivalent circuit of inherent impedance (modified from [35]).

R_a and R_c represent the ohmic resistances of anode and cathode, respectively. R_{cta} and R_{ctc} represent the charge transfer resistances of anode and cathode, respectively. C_{dla} and C_{dlc}, represent the double layer capacitance between anode, cathode and electrolyte.

Similarly, an equivalent circuit of an SOFC can be derived including three parameters. These parameters are ohmic resistance in the inherent impedance; R_o, charge transfer resistance, R_{ct}, and approximated charge transfer capacitance, C_{ct}. In this thesis, the identification of these parameters is made through the result of EIS experiments held at Fuel Cell and Alternative Energy Laboratory at Boğaziçi University. Equivalent circuit of a single SOFC is given in Figure 2.2.

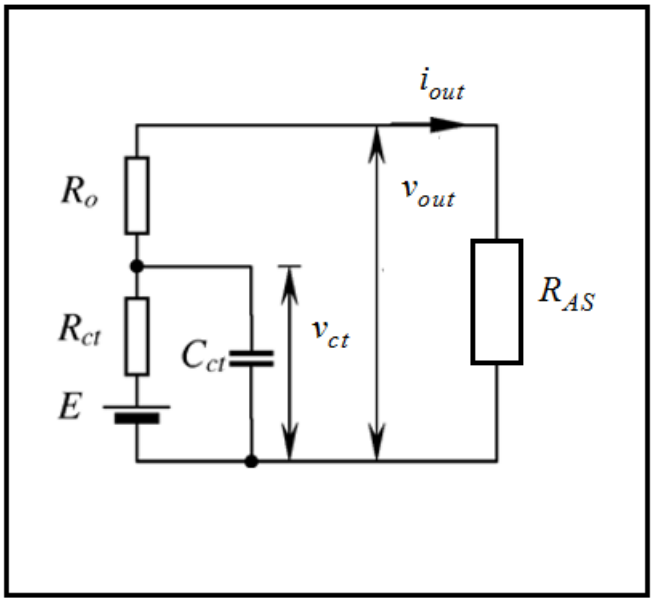


Figure 2.2. Equivalent circuit of a single SOFC.

Thus, the dynamic behavior of the voltage output based on the equivalent circuit is determined by following equations [35]:

$$\dot{v}_{ct} = \frac{1}{R_{ct}\,C_{ct}}E - \frac{1}{R_{ct}C_{ct}}v_{ct} - \frac{1}{C_{ct}}i_{out} \tag{2.27}$$

$$v_{out} = v_{\mathrm{ct}} - i_{out} R_o \tag{2.28}$$

$$i_{out} = \frac{v_{\mathrm{ct}}}{R_o + R_{AS}} \tag{2.29}$$

where v_{out} is output voltage, i_{out} is output current, R_{AS} is the temperature specific ASR value driven from the experimental results, and R_{o} is ohmic resistance.

2.2.6. Model in the State-Space Form

Equation 2.11 and 2.12 are converted to differential equation form to investigate the dynamic behaviors. These dynamic behaviors are hydrogen consumption rate, partial pressure in the vicinity of anode oxygen consumption rate, partial pressure in the vicinity of cathode tpb and are calculated, respectively as follows [35]:

- Hydrogen consumption rate:

$$\ddot{J}^{\mathrm{s}}_{\mathrm{H}_2} = -h_1 J^{\mathrm{s}}_{\mathrm{H}_2} - h_2 \dot{J}^{\mathrm{s}}_{\mathrm{H}_2} + h_1 J^{\mathrm{r}}_{\mathrm{H}_2} + h_3 \frac{A}{RT} \dot{p}^{\mathrm{b}}_{\mathrm{H}_2} \tag{2.30}$$

- Partial pressure in the vicinity of anode tpb:

$$\ddot{p}^{\mathrm{tpb}}_{\mathrm{H}_2} = -h_1 p^{\mathrm{tpb}}_{\mathrm{H}_2} - h_2 \dot{p}^{\mathrm{tpb}}_{\mathrm{H}_2} - h_4 \frac{RT}{A} J^{\mathrm{r}}_{\mathrm{H}_2} - \frac{4}{L_a} \frac{RT}{A} \dot{J}^{\mathrm{r}}_{\mathrm{H}_2} + h_1 p^{\mathrm{b}}_{\mathrm{H}_2} \tag{2.31}$$

where $h_1 = 24 D^2_{\mathrm{H}_2} / L^4_{\mathrm{a}}$, $h_2 = 12 D^2_{\mathrm{H}_2} / L^2_{\mathrm{a}}$, $h_3 = 24 D^2_{\mathrm{H}_2} / L^3_{\mathrm{a}}$ and $h_4 = 24 D^2_{\mathrm{H}_2} / L^3_{\mathrm{a}}$.

- Oxygen consumption rate:

$$\ddot{J}^{s}_{O_2} = -o_1 J^{s}_{O_2} - o_2 \dot{J}^{s}_{O_2} + o_1 J^{r}_{O_2} + o_3 \frac{A}{RT} \dot{p}^{b}_{O_2} \tag{2.32}$$

- Partial pressure in the vicinity of cathode tpb:

$$\ddot{p}^{tpb}_{O_2} = -o_1 p^{tpb}_{O_2} - o_2 \dot{p}^{tpb}_{O_2} - o_4 \frac{RT}{A} J^{r}_{O_2} - \frac{4}{L_c} \frac{RT}{A} \dot{J}^{r}_{O_2} + o_1 p^{b}_{O_2} \tag{2.33}$$

where $o_1 = 24D^2_{O_2} / L^4_c$, $o_2 = 12D^2_{O_2} / L^2_c$, $o_3 = 24D^2_{O_2} / L^3_c$ and $o_4 = 24D^2_{O_2} / L^3_c$.

- Water vapor production rate:

$$\ddot{J}^{s}_{H_2O} = -w_1 J^{s}_{H_2O} - w_2 \dot{J}^{s}_{H_2O} + w_1 J^{r}_{H_2O} + w_3 \frac{A}{RT} \dot{p}^{b}_{H_2O} \tag{2.34}$$

- Partial pressure in the vicinity of anode tpb:

$$\ddot{J}^{s}_{H_2O} = -w_1 J^{s}_{H_2O} - w_2 \dot{J}^{s}_{H_2O} + w_1 J^{r}_{H_2O} + w_3 \frac{A}{RT} \dot{p}^{b}_{H_2O} \tag{2.35}$$

where $w_1 = 24D^2_{H_2O} / L^4_a$, $w_2 = 12D^2_{H_2O} / L^2_a$, $w_3 = 24D^2_{H_2O} / L^3_a$, $w_4 = 24D^2_{H_2O} / L^3_a$.

According to the book named Process Dynamics and Control by Seborg et al. [51], first order derivative of an input variable in the Laplace form can be approximated by defining an approximation factor, *K* which is generally greater than or equal to 10. In this study, approximation factor, *K* is taken as 10. By defining this factor, input variable is put in the differential equation form. Mathematically, the Laplace form mentioned is as follows:

$$sU(s) \approx K\left(1-\frac{1}{\frac{1}{K}s+1}\right)U(s) \tag{2.36}$$

Therefore, in order to start defining the states of the system, intermediate variable variables are defined for H, O and H_2O as $\nu_{H_2,}\nu_{O_2}$ and ν_{H_2O}, respectively. After introducing intermediate variables the state of the system can be defined for derived input and output of the system. The differential equation form is given as:

$$\dot{u} = Ku - y \tag{2.37}$$

$$t = K^2u - Kt \tag{2.38}$$

As a result, input vector can be defined including partial pressure of H_2 in gas flow bulk, $p^{b}_{H_2}$, partial pressure of O_2 in gas flow bulk, $p^{b}_{O_2}$, partial pressure of H_2O in gas flow bulk, $p^{b}_{H_2O}$. As follows:

$$\underline{u}(t) = \begin{bmatrix} p^{b}_{H_2} \\ p^{b}_{O_2} \\ p^{b}_{H_2O} \end{bmatrix} \tag{2.39}$$

Output vector can also be defined, including the output voltage, v_{out} and output current which is expressed as i_{out}. Namely,

$$\underline{y}(t) = \begin{bmatrix} v_{out} \\ i_{out} \end{bmatrix} \tag{2.40}$$

The state vector consists of the 17 state variables defined as follows:

$$x_1 = v_{\mathrm{ct}}, x_2 = J^{\mathrm{s}}_{\mathrm{H}_2}, x_3 = \dot{J}^{\mathrm{s}}_{\mathrm{H}_2}, x_4 = \nu_{\mathrm{H}_2}, x_5 = J^{\mathrm{s}}_{\mathrm{O}_2}, x_6 = \dot{J}^{\mathrm{s}}_{\mathrm{O}_2}, x_7 = \nu_{\mathrm{O}_2},$$

$$x_8 = J^{\mathrm{s}}_{\mathrm{H_2O}}, x_9 = \dot{J}^{\mathrm{s}}_{\mathrm{H_2O}}, x_{10} = \nu_{\mathrm{H_2O}}, \quad x_{11} = p^{\mathrm{tpb}}_{\mathrm{H}_2}, x_{12} = \dot{p}^{\mathrm{tpb}}_{\mathrm{H}_2}, x_{13} = p^{\mathrm{tpb}}_{\mathrm{O}_2},$$

$$x_{14} = \dot{p}^{\mathrm{tpb}}_{\mathrm{O}_2}, x_{15} = p^{\mathrm{tpb}}_{H_2O}, x_{16} = \dot{p}^{\mathrm{tpb}}_{\mathrm{H_2O}}, x_{17} = \nu_R. \tag{2.41}$$

The equations in Equation (2.42) are combined to model the system in state-space form. So, the state-space model is given by:

$$\dot{x}_1 = \frac{1}{R_{ct}C_{ct}}E - \frac{1}{R_{ct}C_{ct}}x_1 - \frac{1}{C_{ct}}\frac{1}{A_{SR}+R_o} \tag{2.42}$$

$$\dot{x}_2 = x_3 \tag{2.43}$$

$$\dot{x}_3 = -h_1x_2 - h_2x_3 + h_1\frac{1}{2\mathrm{F}}\frac{x_1}{A_{SR}+R_o} + h_3\frac{A}{RT}(Ku_1 - x_4) \tag{2.44}$$

$$\dot{x}_4 = K^2u_1 - Kx_4 \tag{2.45}$$

$$\dot{x}_5 = x_6 \tag{2.46}$$

$$\dot{x}_6 = -o_1x_5 - o_2x_6 + o_1\frac{1}{4\mathrm{F}}\frac{x_1}{R_{AS}+R_o} + o_3\frac{A}{RT}(Ku_2 - x_7) \tag{2.47}$$

$$\dot{x}_7 = K^2u_2 - Kx_7 \tag{2.48}$$

$$\dot{x}_8 = x_9 \tag{2.49}$$

$$\dot{x}_9 = -w_1x_8 - w_2x_9 + w_1\frac{1}{2\mathrm{F}}\left(\frac{-x_1}{R_{AS}+R_o}\right) + w_3\frac{A}{RT}(Ku_3 - x_{10}) \tag{2.50}$$

$$\dot{x}_{10} = K^2u_3 - Kx_{10} \tag{2.51}$$

$$\dot{x}_{11} = x_{12} \tag{2.52}$$

$$\dot{x}_{12} = -h_1 x_{11} - h_2 x_{12} - h_4 \frac{RT}{A}\frac{1}{2\mathrm{F}}\frac{x_1}{R_{AS}+R_o} - \frac{RT}{A}\frac{4}{L_a}\frac{1}{2\mathrm{F}}\left[\frac{\dot{x}_1}{R_{AS}+R_o} - \frac{x_1}{\left(R_{AS}+R_o\right)^2}\left(KR_{AS}-x_{17}\right)\right] + h_1 u_1 \tag{2.53}$$

$$\dot{x}_{13} = x_{14} \tag{2.54}$$

$$\dot{x}_{14} = -o_1 x_{13} - o_2 x_{14} + o_4 \frac{RT}{A}\frac{1}{4\mathrm{F}}\frac{x_1}{R_{AS}+R_o} - \frac{RT}{A}\frac{4}{L_c}\frac{1}{4\mathrm{F}}\left[\frac{\dot{x}_1}{R_{AS}+R_o} - \frac{x_1}{(R_{AS}+R_o)^2}(KR_{AS}-x_{17})\right] + o_1 u_2 \tag{2.55}$$

$$\dot{x}_{15} = x_{16} \tag{2.56}$$

$$\dot{x}_{16} = -w_1 x_{15} - w_2 x_{16} + w_4 \frac{RT}{A}\frac{1}{2\mathrm{F}}\left(\frac{-x_1}{R_{AS}+R_o}\right) - \frac{RT}{A}\frac{4}{L_a}\frac{1}{2\mathrm{F}}\left[-\frac{\dot{x}_1}{R_{AS}} + \frac{x_1}{(R_{AS}+R_o)^2}(KR_{AS}-x_{17})\right] + w_1 u_3 \tag{2.57}$$

$$\dot{x}_{17} = K^2 R_{AS} - K x_{17} \tag{2.58}$$

Output vector is as follows:

$$\underline{\mathrm{y}}(t) = \begin{bmatrix} \mathrm{y}_1(\mathrm{t}) \\ \mathrm{y}_2(\mathrm{t}) \end{bmatrix} = \begin{bmatrix} 1 - \dfrac{R_{AS}}{R_{AS}+R_o} \\ \dfrac{1}{R_{AS}+R_o} \end{bmatrix} x_1 = \begin{bmatrix} v_{out}(\mathrm{t}) \\ i_{out}(\mathrm{t}) \end{bmatrix} \tag{2.59}$$

State equations and output equations are as follows:

$$\dot{\underline{\mathrm{x}}}(\mathrm{t}) = \underline{\mathrm{F}}(\underline{\mathrm{x}}(\mathrm{t}), \underline{\mathrm{u}}(\mathrm{t})) = \underline{\mathrm{f}}(\underline{\mathrm{x}}(\mathrm{t})) + \underline{\underline{\mathrm{B}}}\underline{\mathrm{u}}(\mathrm{t}) \tag{2.60}$$

In our case, the equations that $\underline{\mathrm{f}}(\underline{\mathrm{x}})$ consists of is given from Eq. 2.42 to Eq. 2.58.

3. RESULTS and DISCUSSION

3.1. Model Parameters

In this part of the study, the parameters used in computer simulations are monitored. The results of the experiments held at Fuel Cells and Energy Laboratory at Boğaziçi University are considered as some of the parameters in this work.

The three dimensional figure of the planar SOFC which is fabricated and operated at Fuel Cells and Energy Laboratory at Boğaziçi University is presented in Figure 3.1. The arrows on the figure represents the movement directions of the species. According to the figure, the definition of the elemental volume in planar SOFC is given. In this study, it is assumed that the temperature distribution is uniform. Therefore, consideration of elemental volume allows to observe the dynamic behaviour of planar SOFC under uniform temperature conditions.

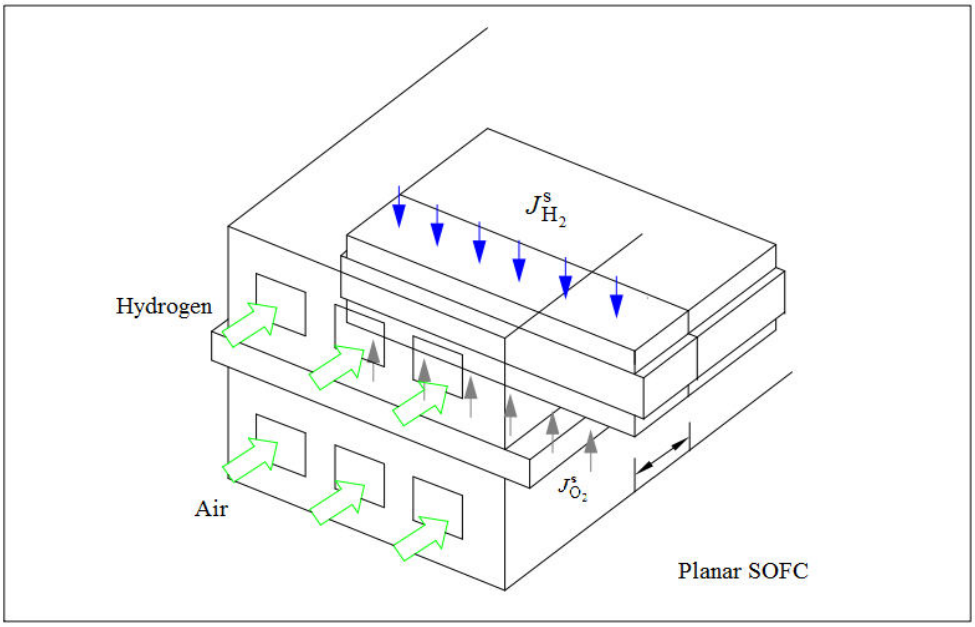


Figure 3.1. Schematic representation of a planar SOFC fabricated at Fuel Cells and Energy Laboratory in Boğaziçi University (drawing is not to scale).

The performance of a planar SOFC system is investigated by using state-space equations conducted in dynamic modeling on basis of simulations held on a MATLAB®

software platform by using the parameters given above. The operating temperature of the planar SOFC fabricated is from 400°C to 800°C with an increment of 50°C.

Table 3.1. Parameters used in simulation.

Symbol	**Description**	**Source**
$L_a = 1$	Thickness of anode diffusion layer	Fuel Cells and Energy Laboratory
$L_c = 1$	Thickness of cathode diffusion layer	Fuel Cells and Energy Laboratory
$A = 1\ cm^2$	Fuel cell effective area	Fuel Cells and Energy Laboratory
R_{ct} (Ω)	Charge transfer resistance	EIS tests held at Fuel Cells and Energy Laboratory (given in Table 3.3)
R_o (Ω)	Ohmic resistance	EIS tests held at Fuel Cells and Energy Laboratory (given in Table 3.2)
$E_{act,a}$	Anode activation energy	Campanari et al. [41]
$E_{act,c}$	Cathode activation energy	Campanari et al. [41]
C (F)	Charge transfer capacitance	EIS tests held at Fuel Cells and Energy Laboratory (given in Table 3.4)

Diffusional volume is a distinctive property of a substance. The diffusional volume of H_2, H_2O, O_2 and N_2 are given in Table 3.2 and used as some of the parameters of this

modeling study. In addition, tortuosity, τ value and porosity ε value is taken from Welty et al [45].

Table 3.2. Diffusional volume parameters.

Symbol	Description	Source
$(\sum_{i=1}^{2} v_i)H_2 = 7.07$	Diffusional Volume of H_2	Welty et al. [45]
$(\sum_{i=1}^{2} v_i)H_2O = 12.7$	Diffusional Volume of H_2O	Welty et al. [45]
$(\sum_{i=1}^{2} v_i)O_2 = 16.6$	Diffusional Volume of O_2	Welty et al. [45]
$(\sum_{i=1}^{2} v_i)N_2 = 17.9$	Diffusional Volume of N_2	Welty et al. [45]

Partial pressure values are used as the input parameters of this modeling study. In order to see the effect of the amount of H_2 supplied as fuel, two different partial pressure values of H_2 is taken into account and the output results of the simulations are compared. Partial pressure values are represented in Table 3.3.

Table 3.3. Partial pressure values used in simulation.

Symbol	Description	Source
$p^b_{H_2}$ = 0.54, 0.27	Partial Pressure of H_2	LSV tests
$p^b_{H_2O}$ = 0.03	Partial Pressure of water	LSV tests
$p^b_{O_2}$ = 0.18	Partial Pressure of O_2	LSV tests

Ohmic resistance, R_o (Ω) values of YSZ at different temperatures and hydrogen partial pressures are characteristic property of EIS results held at Fuel Cell and Energy laboratory. Therefore, these empirical results are taken as R_o (Ω) values in this modeling study and given in Table 3.4.

Table 3.4. Ohmic resistance, R_o (Ω) values of YSZ at different temperatures and hydrogen partial pressures.

YSZ	400°C	450°C	500°C	550°C	600°C	650°C	700°C	750°C	800°C
H_2(0.27)	3.6	2.6	1.37	1.63	0.76	0.47	0.36	0.27	0.14
H_2(0.54)	2.5	1.9	1.25	1.41	0.7	0.35	0.28	0.21	0.09

Charge transfer resistance, R_{ct} (Ω) values of YSZ at different temperatures and hydrogen partial pressures are characteristic property of EIS results held at Fuel Cell and Energy laboratory. Therefore, these empirical results are taken as R_{ct} (Ω) values in this modeling study and given in Table 3.5.

Table 3.5. Charge transfer resistance, R_{ct} (Ω) values of YSZ at different temperatures and hydrogen partial pressures.

YSZ	400°C	450°C	500°C	550°C	600°C	650°C	700°C	750°C	800°C
H_2(0.27)	31.74	23.2	15.08	4.692	2.8	1.95	1.32	0.627	0.594
H_2(0.54)	31.56	23.8	10.47	4.624	2.08	1.85	1.309	0.619	0.528

Charge transfer capacitance, C_{ct} (Ω) values of YSZ at different temperatures and hydrogen partial pressures are characteristic property of EIS results held at Fuel Cell and Energy laboratory. Therefore, these empirical results are taken as C_{ct} (F) values in this modeling study and given in Table 3.5.

Table 3.6. Charge transfer capacitance, C (Farad) values of YSZ at different temperatures and hydrogen partial pressures.

YSZ	400°C	450°C	500°C	550°C	600°C	650°C	700°C	750°C	800°C
H_2(0.27)	15.87	11.6	7.54	2.346	1.4	0.975	0.66	0.3135	0.297
H_2(0.54)	15.78	11.9	5.235	2.312	1.04	0.925	0.655	0.27	0.264

It should be noted that the output current is directly affected by the area specific resistance value, R_{AS}, which needs to be included as a parameter in the dynamic model. The value of R_{AS}, can be obtained either empirically or EIS simulation results. Area

specific resistance value is often expressed as ASR, shortly. In this thesis, empirical values of R_{AS} has been used as the parameter value in the dynamic model.

Table 3.7. Area Specific Resistance, ASR (Ω) values of YSZ at different temperatures and hydrogen partial pressures.

YSZ	400°C	450°C	500°C	550°C	600°C	650°C	700°C	750°C	800°C
H_2(0.27)	33.84	25.9	12.608	10.872	8.78	5.85	3.32	0.659	0.730
H_2(0.54)	33.56	25.73	12.402	10.524	8.42	4.80	3.10	0.643	0.689

3.2. Comparison of Simulated Planar SOFC Performance Test Results with Empirical Performance Test Results

The computer simulation of the model is performed. Performance tests and voltage-current-power (V-I-P) values are obtained. Performance of fuel cell as a combination of voltage-current density and power density-current density graphs are displayed by comparing the performances of the planar SOFC operated at Fuel Cells and Energy Laboratory at Boğaziçi University and simulation results of the cell for nine different temperatures varying from 400°C to 800°C with an increment of 50°C. The maximum point on the power density curve gives information about the performance of the cell. To make a comprehensive comparison between the empirical results and simulation results, the same operating parameters are taken into account.

As it can be seen in Figure 3.2, the maximum power density of the planar cell operated is about 0.00084 W/cm^2. According to simulation results, the maximum power density of the cell is 0.00099 W/cm^2. In other words, the maximum power of the experimental result is 17.86% less than the maximum power of the simulation results. The reason for this difference is that during the experiment, Open Current Voltage (OCV) decreased due to experimental errors while operating the cell. In addition, according to Figure 3.2 the cell operated reaches to expected current density values in the experiments. However, the cell current density and power density difference are not remarkable for the

experimental and simulation results. It can be said that there is a correlation between experimental results and simulation results at 400°C.

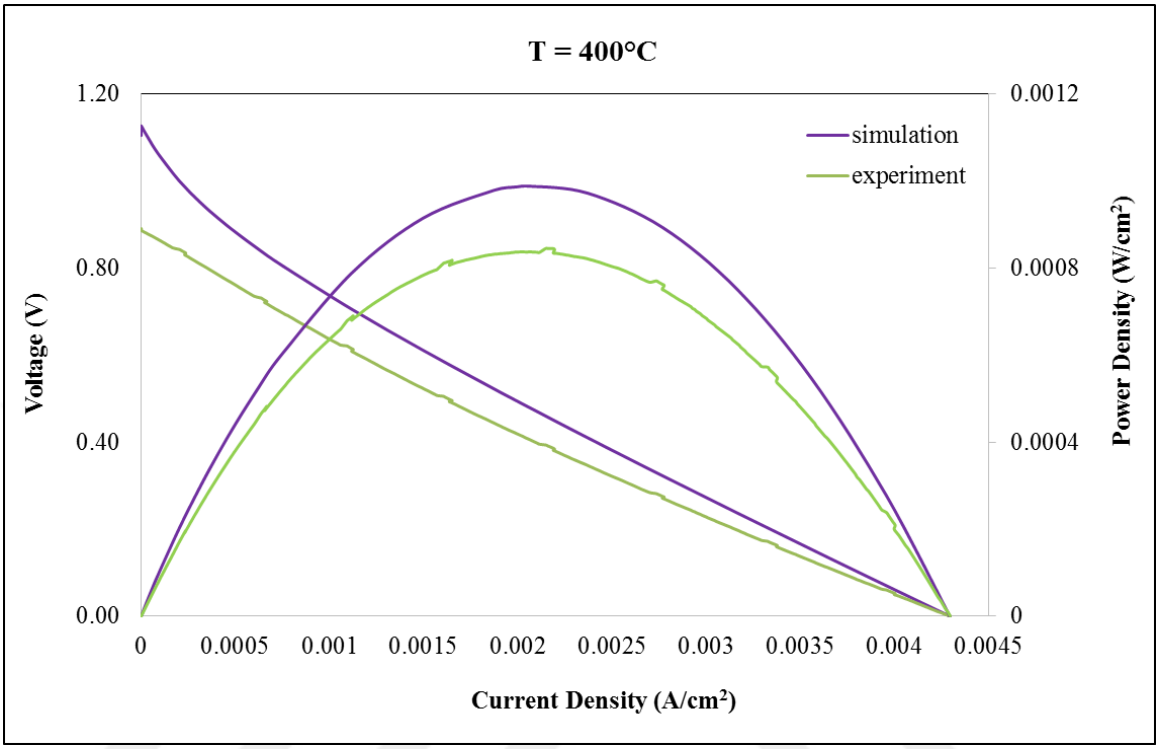


Figure 3.2. Comparison of fabricated and operated planar SOFC at Fuel Cells and Energy Laboratory and modeled planar SOFC in terms of voltage, current density and power density at 400°C. (simulation: V-I-P curve of simulation results at 400°C, experiment: V-I-P curve of experimental results at 400°C where partial pressure of H_2 is 0.54)

Figure 3.3 represents that the maximum power density of the planar cell operated is about 0.00167 W/cm^2. According to simulation results, the maximum power density of the cell is 0.0014 W/cm^2. In other words, the maximum power of the experimental result is 16.17% less than the maximum power of the simulation results. The reason for this difference is that during the experiment, Open Current Voltage (OCV) decreased due to experimental errors while operating the cell. In addition, according to Figure 3.3 cell operated reaches to expected current density values in the experiments. However, the cell current density and power density difference are not remarkable for the experimental and simulation results. It can be said that there is a correlation between experimental results and simulation results at 450°C.

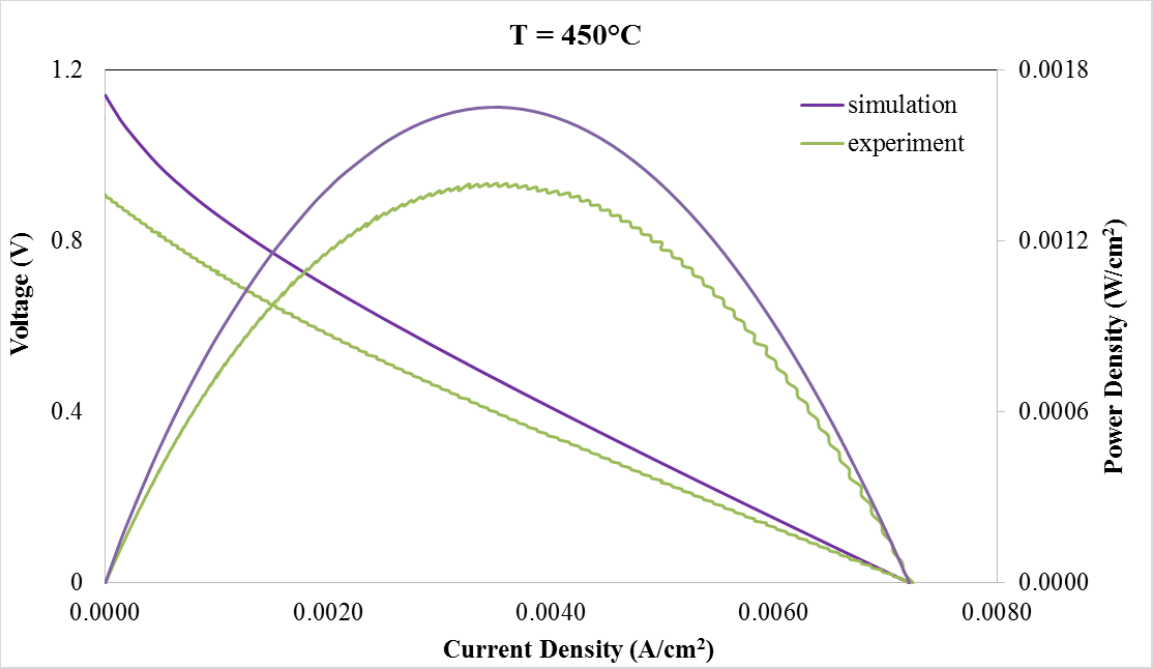


Figure 3.3. Comparison of fabricated and operated planar SOFC at Fuel Cells and Energy Laboratory and modeled planar SOFC in terms of voltage, current density and power density at 450°C. (simulation: V-I-P curve of simulation results at 450°C, experiment: V-I-P curve of experimental results at 450°C where partial pressure of H_2 is 0.54)

In Figure 3.4, the maximum power density of the planar cell operated is about 0.00302 W/cm^2. According to simulation results, the maximum power density of the cell is 0.00286 W/cm^2. In other words, the maximum power of the experimental result is 5.3% more than the maximum power of the simulation results. In addition, according to Figure 3.4 the cell operated reaches to expected current density values in the experiments. However, the cell current density and power density difference are not remarkable for the experimental and simulation results. It can be said that there is a correlation between experimental results and simulation results at 500°C.

In Figure 3.4, the maximum power density of the planar cell operated is about 0.00302 W/cm^2. According to simulation results, the maximum power density of the cell is 0.00286 W/cm^2. In other words, the maximum power of the experimental result is 5.3% more than the maximum power of the simulation results. In addition, according to Figure 3.4 the cell operated reaches to expected current density values in the experiments.

However, the cell current density and power density difference are not remarkable for the experimental and simulation results. It can be said that there is a correlation between experimental results and simulation results at 500°C.

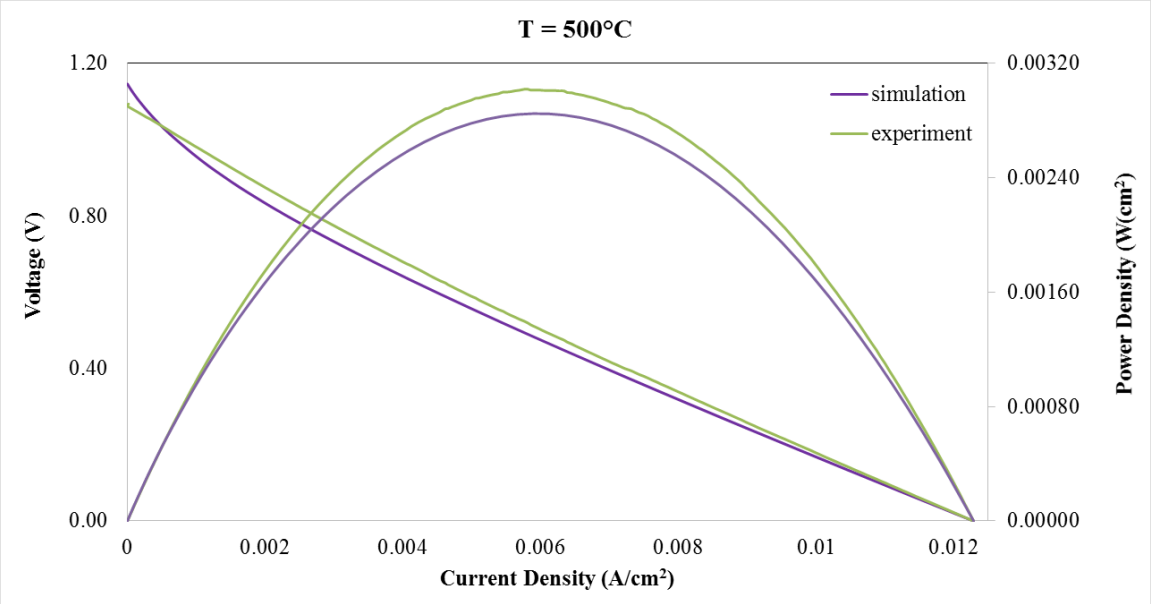


Figure 3.4. Comparison of fabricated and operated planar SOFC at Fuel Cells and Energy Laboratory and modeled planar SOFC in terms of voltage, current density and power density at 500°C. (simulation: V-I-P curve of simulation results at 500°C, experiment: V-I-P curve of experimental results at 500°C where partial pressure of H_2 is 0.54)

Figure 3.5 represents that the maximum power density of the planar cell operated is about 0.004 W/cm^2. According to simulation results, the maximum power density of the cell is also 0004 W/cm^2. These values prove that simulation and experimental results match perfectly. The reason for this improvement is that the experimental error is almost equal to 0. In addition, the experimental results are almost equal to the expected results. Under this operating conditions, it can be considered as the cell is operating almost without an error at 550°C.

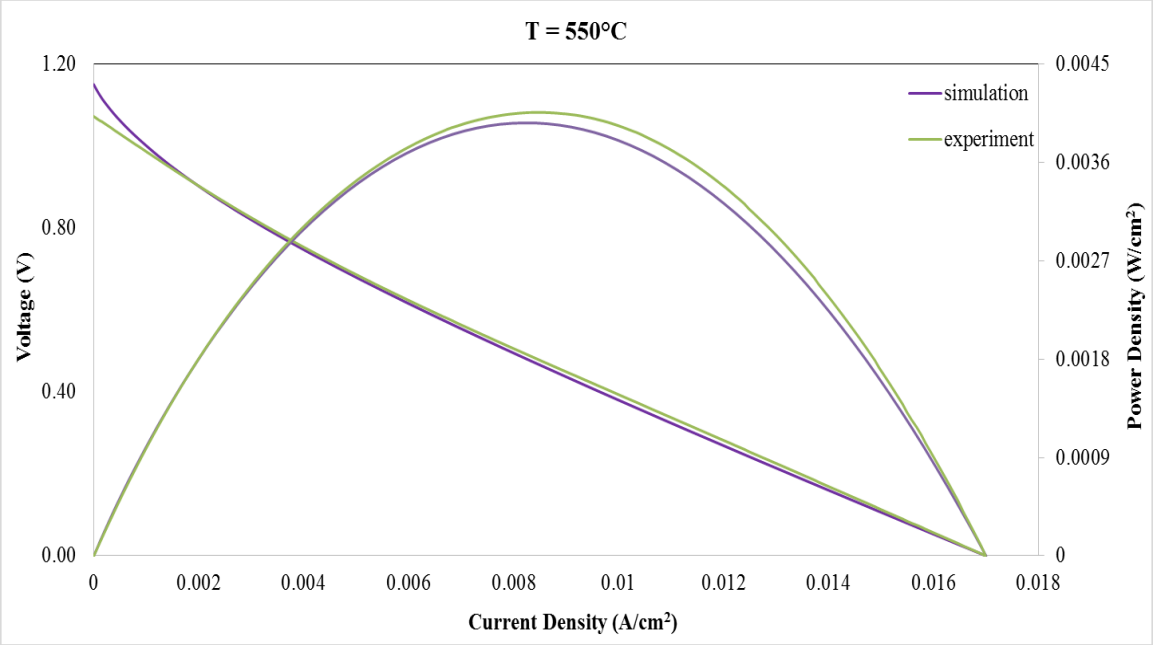


Figure 3.5. Comparison of fabricated and operated planar SOFC at Fuel Cells and Energy Laboratory and modeled planar SOFC in terms of voltage, current density and power density at 550°C. (simulation: V-I-P curve of simulation results at 550°C, experiment: V-I-P curve of experimental results at 550°C where partial pressure of H_2 is 0.54)

Figure 3.6 represents that the maximum power density of the planar cell operated is about 0.0048 W/cm^2. According to simulation results, the maximum power density of the cell is 0.0045 W/cm^2. In other words, the maximum power of the experimental result is almost equal to the maximum power of the simulation results. In addition, according to Figure 3.6 the cell operated reaches to expected current density values in the experiments. However, the cell current density and power density difference are not remarkable for the experimental and simulation results. It can be said that there is a correlation between experimental results and simulation results at 600°C.

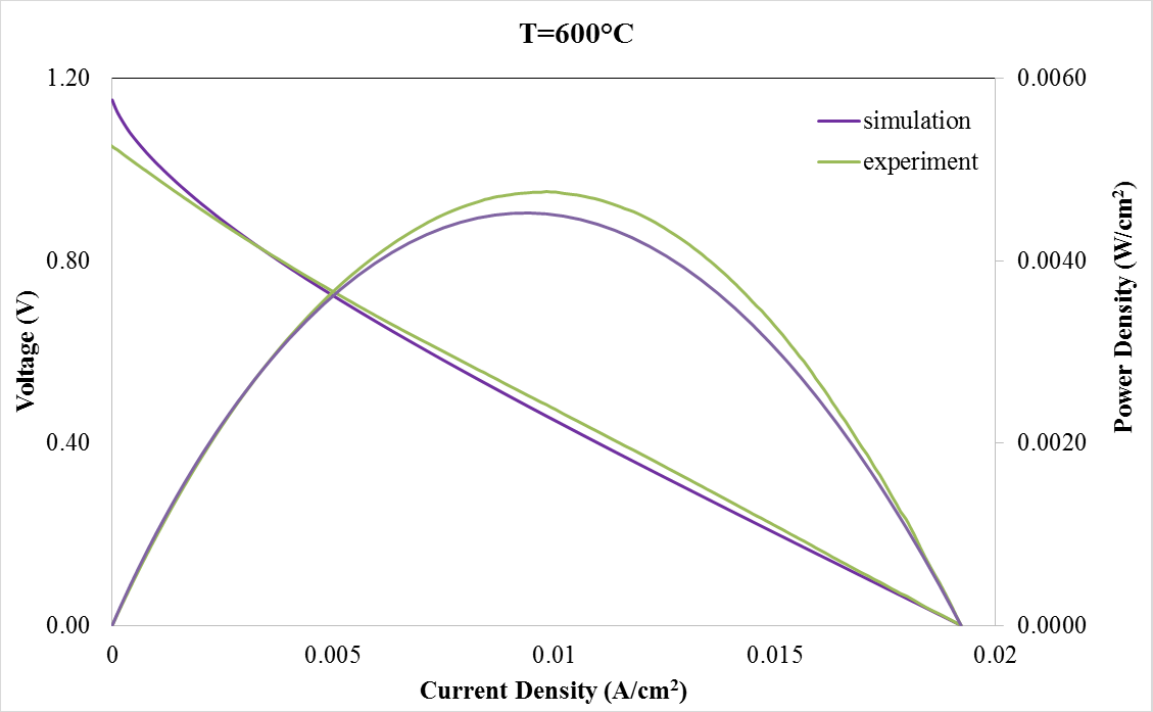


Figure 3.6. Comparison of fabricated and operated planar SOFC at Fuel Cells and Energy Laboratory and modeled planar SOFC in terms of voltage, current density and power density at 600°C. (simulation: V-I-P curve of simulation results at 600°C, experiment: V-I-P curve of experimental results at 600°C where partial pressure of H_2 is 0.54)

Figure 3.7 represents that the maximum power density of the planar cell operated is about 0.006 W/cm^2. According to simulation results, the maximum power density of the cell is 0.00574 W/cm^2. In other words, the maximum power of the experimental result is 4.33% more than the maximum power of the simulation results. In addition, according to Figure 3.7 the cell operated reaches to expected current density values in the experiments. However, the cell current density and power density difference are not remarkable for the experimental and simulation results. It can be said that there is a correlation between experimental results and simulation results at 650°C.

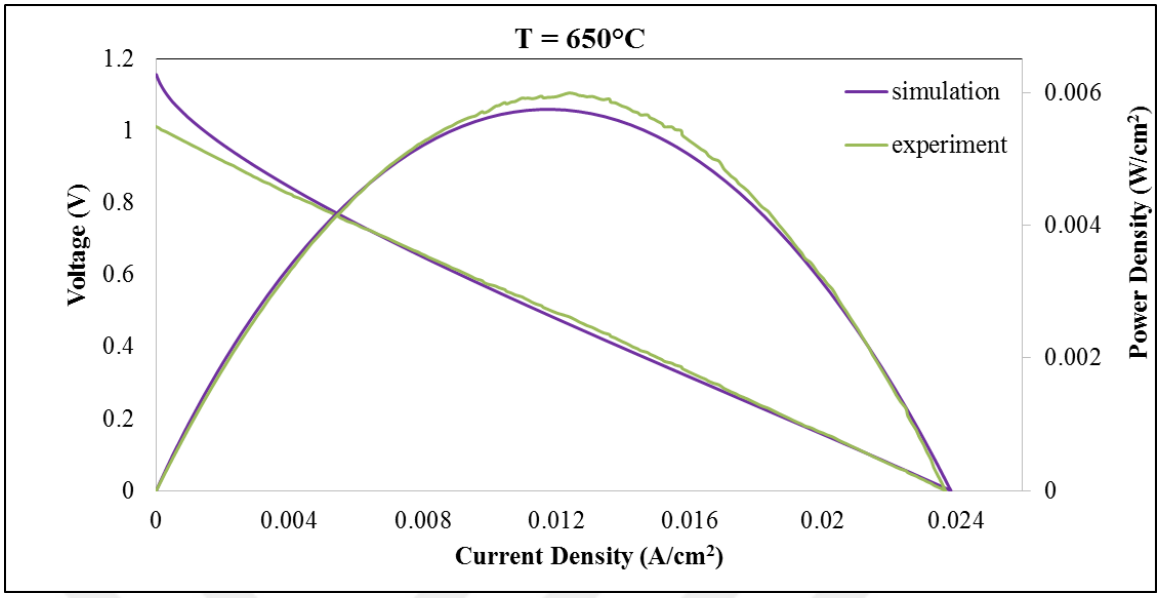


Figure 3.7. Comparison of fabricated and operated planar SOFC at Fuel Cells and Energy Laboratory and modeled planar SOFC in terms of voltage, current density and power density at 650°C. (simulation: V-I-P curve of simulation results at 650°C, experiment: V-I-P curve of experimental results at 650°C where partial pressure of H_2 is 0.54)

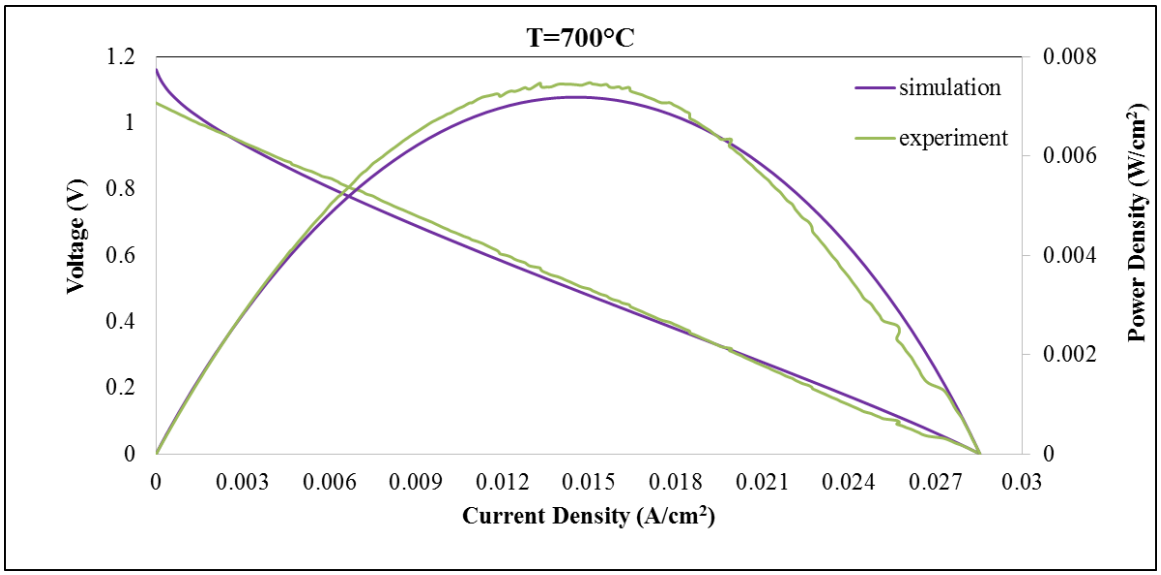


Figure 3.8. Comparison of fabricated and operated planar SOFC at Fuel Cells and Energy Laboratory and modeled planar SOFC in terms of voltage, current density and power density at 700°C. (simulation: V-I-P curve of simulation results at 700°C, experiment: V-I-P curve of experimental results at 700°C where partial pressure of H_2 is 0.54)

The experiments held at 750°C and 800°C failed due to experimental errors. However, there is another experiment held at 800°C and given in Figure 3.9 Simulation results at conducted at 750°C and 800°C are given in the next chapter.

In this chapter, experimental results are normalized with respect to the area of the planar SOFC.

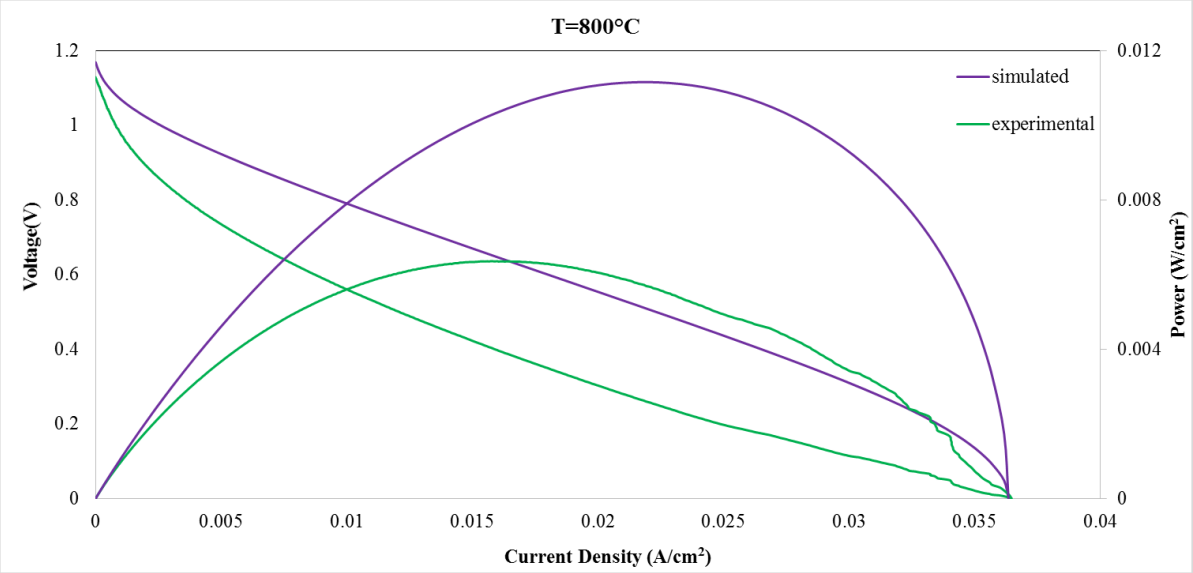


Figure 3.9. Comparison of another fabricated and operated planar SOFC at Fuel Cells and Energy Laboratory and modeled planar SOFC in terms of voltage, current density and power density at 800°C. (simulation: V-I-P curve of simulation results at 800°C, experiment: V-I-P curve of experimental results at 800°C where partial pressure of H_2 is 0.54).

As it can be seen in the graph, the maximum power density of the experiment on the cell is 0.0055 W/cm^2. The simulation result at 800°C represents that the maximum power density is 0.01116 W/cm^2. This means that the maximum power density value of the simulation results is 55% more than the maximum power density value of the experimental results. However, the external factors at experiments are not considered in the simulations and both experimental and simulation results are reasonable.

In this work, the planar SOFC is modeled under ideal conditions. The model can be used to explore the effects of the catalytical (activation time, charge transfer parameter and surface diffusion parameter) and physical (parameters conductivity and morphology of the

cell such as particle size, grain size and pore size) parameters on the SOFC performance prior to experimentation, and optimize them. Of course, these parameters may still need to be fine-tuned in experiments because of approximation errors. According to the differences in OCV values of the simulation results and experimental results, it can be seen that there is a leakage of H_2O or O_2 during the experiment.

3.3. Simulated Planar SOFC Performance Test Results with different H_2 operating Parameters

In this section, the effect of changes in partial pressure of the fuel, H_2 is investigated. At the beginning of the experiments, the partial pressure of H_2 is 0.54. However, as the reactions occur and the fuel starts to operate, the fuel is consumed. Therefore, the partial pressure of the fuel is reduced. It means that there is a direct relation between the amount of the partial pressure and the current produced. In order to observe this, there are two different simulations conducted. Namely, at the first simulation group conducted at held at temperatures from 400°C to 800°C with an increment of 50°C, the partial pressure of H_2 is 0.54. At the second simulation group held at temperatures from 400°C to 800°C with an increment of 50°C, the partial pressure of H_2 is 0.27. By changing the amount of the partial pressure, it is aimed to check whether the response of the model is changing or not. It can be seen from the graphs that the model responds to the following changes.

Figure 3.10 represents that when the partial pressure of H_2 is 0.54, the maximum current density of the simulation of the cell is 0.00429 A/cm^2. However, when partial pressure of H_2 is 0.27, the simulation results yield that the maximum current density is 0.00367 A/cm^2. This shows that the model responds to the changes in partial pressure. In other words, when the H_2 is supplied to operate the cell, it can be seen that there is a correlation between the amount of the partial pressure and the current produced.

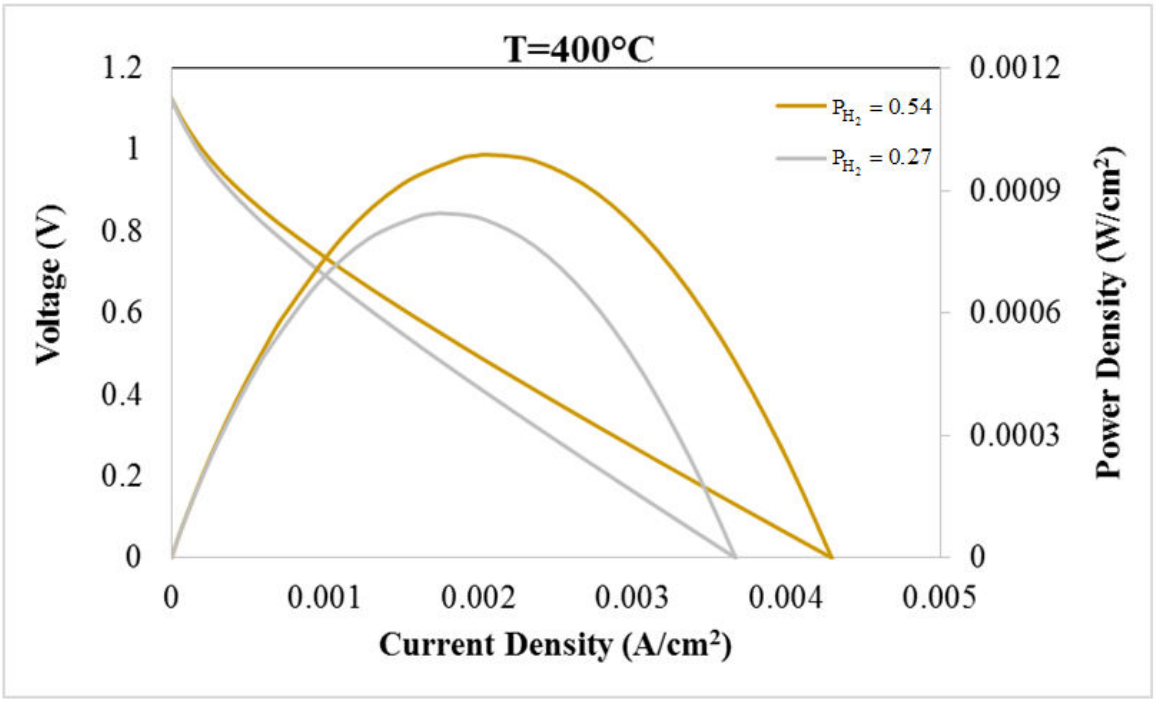


Figure 3.10. Comparison of simulated planar SOFC at different partial pressures of H_2 in terms of voltage, current density and power density at 400°C. (P_{H_2}=0.54: V-I-P curve of simulation results at 400°C, 0.54 is taken as H_2 partial pressure, P_{H_2}=0.27: V-I-P curve of simulation results at 400°C, 0.27 is taken as H_2 partial pressure)

Figure 3.11 represents the entire working temperature intervals for partial pressure of H_2 as 0.54. It can be seen that as the temperature increases, the current density also increases. In addition, Figure 3.12 represents the entire working temperature intervals for partial pressure of H_2 as 0.27. It is observed that as the temperature increases, the current density also increases. However, as it is mentioned before, the current density results at lower partial pressure value, 0.27 is lower than the current density results at partial pressure of 0.54.

As it can be seen from Figure 3.11 and 3.12, the model responds to the effect of partial pressure of the fuel, H_2. Since the partial pressure of H_2 is reduced to half of it, there must be a 20% of decrease in each of the current density values for all temperature values that the simulation is conducted. However, in the model, this difference ranges between 15% to 40% for different temperature regions. Therefore, the model should be optimized at these regions by considering the characteristic of the materials used.

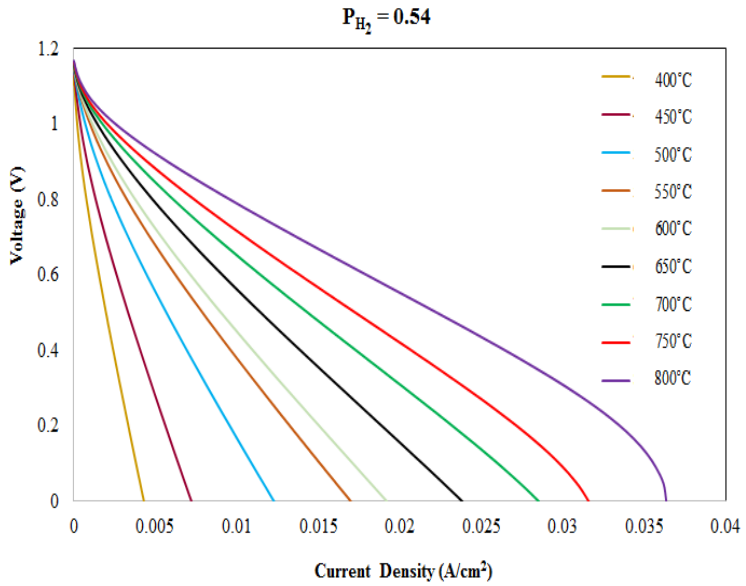


Figure 3.11. Simulated planar SOFC at different partial pressure of H_2 as 0.54 in terms of voltage and current density at the temperature ranges between 400°C to 800°C with an increment of at 50°C.

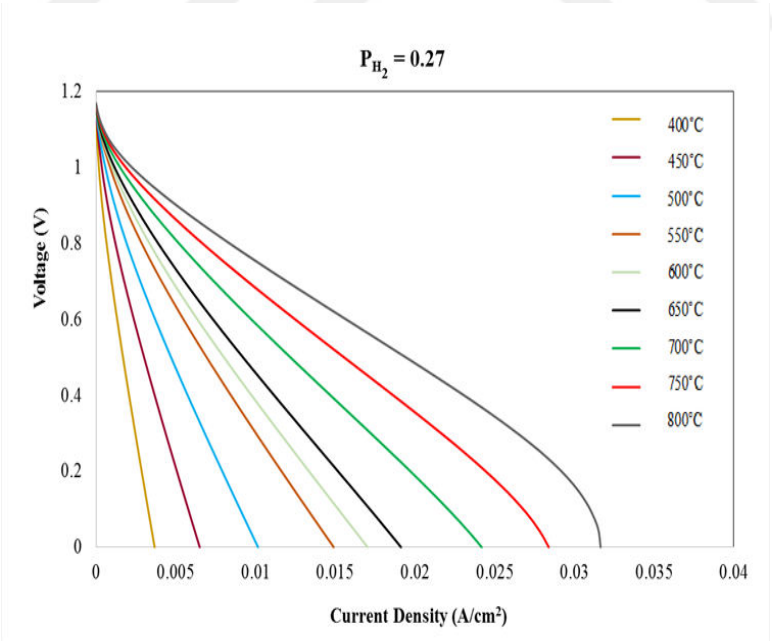


Figure 3.12. Simulated planar SOFC at different partial pressure of H_2 as 0.27 in terms of voltage and current density at the temperature ranges between 400°C to 800°C with an increment of at 50°C.

4. CONCLUSION

At Fuel Cells and Alternative Energy Laboratory at Boğaziçi University, the researches on developing high quality materials for various temperature SOFCs have been continued. Measurements on performance of the planar SOFC are held via LSV and EIS. In this thesis, the performance of a planar SOFC system is investigated on basis of simulations conducted on a MATLAB® software platform by using dynamic modeling approach. The model equations serve as basis for a computer simulation of the planar SOFC operation by using some of the experimental parameters derived from Fuel Cells and Alternative Energy Laboratory.

In this research, the mathematical model is applied in a complete fuel cell system model. Several simulations of the dynamic system have been performed from 400^0C to 800^0C as operating temperature. To make a comprehensive comparison between the empirical and simulation results, the setting of parameters on mathematical model are taken from empirical EIS results and LVS results. The validity of the model is checked through these comparisons. The maximum power and current densities are investigated and compared between both experimental and simulation studies.

Conducting the comparison studies between empirical and simulation results, when the current and power densities are normalized with respect to the interface area between Ni and YSZ, it can be seen from the results that the current and power densities are almost identical within acceptable experimental errors.

This work allows us to observe the influence of various parameters to operate planar SOFC and to determine the limiting factors of the considered planar SOFC mechanism. In addition, the model helps to investigate the experimental results conducted at Fuel Cells and Energy Laboratory at Boğaziçi University.

The approach proposed in this study is reliable due to the changes in parameters; temperature and input variable, such as partial pressure of the fuel, H_2 added. By observing

the changes in input variable, namely partial pressure of H_2, it can be seen that the model also responses to time-variant changes.

Lastly, this modelling study is a unique representation of a real-time experiments conducted at Fuel Cells and Energy Laboratory at Boğaziçi University. The purpose of this modeling study is to investigate the effects of different materials by considering their chemical and physical properties to operate a planar SOFC.

5. FUTURE WORK

In addition to computational modeling of SOFC performance tests for conventional planar SOFC (Ni-YSZ anode, YSZ electrolyte, LSM-YSZ cathode) held at this study by considering H_2 as the fuel, new modeling study can be conducted for hydrocarbons as fuel.

By working cooperatively with material scientists, the scope of the model can be expanded by considering the expansion rates of the materials as the temperature is increased.

The model explained in this study can be compared with the modeling study that uses finite element methods as modeling approach.

EIS modeling study can be derived to investigate the performance analyses together with this modeling study.

New modeling study can be conducted for tubular SOFC to compare the advantages and drawbacks of various fuel cell types under different operation parameters.

The scope of the model can be expanded by simulating the results for the fuel, H_2 and oxygen consumption rate.

6. REFERENCES

1. Badwal, S., Solid oxide electrolyte fuel cell review, *Ceramics International, 22*(3), 257-265, 1996.

2. Huang, K., Introduction to solid oxide fuel cells (SOFCs), *Solid Oxide Fuel Cell Technology,* 1-9, 2009.

3. Sira, T., Solid oxide fuel cells, *The Electrochemical Society Proceedings Series*, PV 93-4, 1993.

4. lesner, R., "Modeling of Solid Oxide Fuel Cell functionally graded electrodes and a feasibility study of fabrication techniques for functionally graded electrodes", Graduate Theses and Dissertations, Paper 11063, 2009.

5. Li, X., "Principles of Fuel Cells", *Taylor & Francis Group*, 2-7, 2006.

6. Jain, R., "Studies on Ideal and Actual Efficiency of Solar Polymer Electrolyte Fuel Cell", 2007.

7. Aaron, D., Tang, Z., Papandrew, A. B., and Zawodzinski, T. A., "Polarization curve analysis of all-vanadium redox flow batteries", *Journal of Applied Electrochemistry*, 41(10), 1175-1182, 2011.

8. Minh, N. Q., "Solid Oxide Fuel Cell Technology-Features and Applications", Solid State Ionics, 174(1-4), pp. 271-277., 2007.

9. Reiss, H., "*Methods of Thermodynamics"*, Dover Publications, 1965.

10. Peter A., *Chemical Principles: The Quest for Insight*. W. H. Freeman, 2007.

11. Gibbs, J.W., "A Method of Geometrical Representation of the Thermodynamic Properties of Substances by Means of Surfaces", *Transactions of the Connecticut Academy of Arts and Sciences 2*, 1873.

12. Shapiro, N.Z., "Mass Action Laws and the Gibbs Free Energy Function", *Journal of the Society for Industrial and Applied Mathematics*, 13(2), 353–375.

13. Larminie J., "Fuel Cell Systems Explained", *John Wiley & Sons Inc.*, 2003.

14. Hahn A., Landes H., "Investigations into the kinetics of SOFC cathodes", *The Electrochemical Society*, 1997.

15. Okumura K., Yamamoto Y., Fukui T., Hanyu S., Kubo Y., Esaki Y., Hattori M., Kusunoki A. and Takeuchi S., "Microstructure and overvoltage characteristics of the anode for Solid Oxide Fuel Cells", *Proc. Of the 3rd Int. Symp. On Solid Oxide Fuel Cells*, pp. 444-53, 1993.

16. Gu, W., Wu, Z., Bo, R., Liu, W., Zhou, G., Chen, W., and Wu, Z., "Modeling, planning and optimal energy management of combined cooling, heating and power microgrid: A review", *International Journal of Electrical Power & Energy Systems*, 54, 26-37, 2014.

17. Hamnett, A., "Mechanism and electrocatalysis in the direct methanol fuel cell", *Catalysis Today*, 38.4: 445-457, 1997.

18. Andersson, M., Yuan, J., and Sundén, B., "SOFC modeling considering electrochemical reactions at the active three phase boundaries", *International journal of heat and mass transfer*, 55(4), 773-788., 2012.

19. Andersson, M., Yuan, J., and Sundén, B., "SOFC modeling considering hydrogen and carbon monoxide as electrochemical reactants", *Journal of Power Sources*, 232, 42-54, 2013.

20. Kandepu, R., Imsland, L., Foss, B. A., Stiller, C., Thorud, B., and Bolland, O., "Control-relevant SOFC modeling and model evaluation", *Proceedings of ECOS*, 2005.

21. Lazzaretto, A., Toffolo, A., and Zanon, F., "Parameter setting for a tubular SOFC simulation model", *Journal of energy resources technology*, 126(1), 40-46, 2004.

22. Leonide, A., Apel, Y., and Ivers-Tiffee, E., "SOFC modeling and parameter identification by means of impedance spectroscopy", *ECS Transactions*, 19(20), 81-109, 2004.

23. Ellis, M. W., Von Spakovsky, M. R., and Nelson, D. J., "Fuel cell systems: efficient, flexible energy conversion for the 21st century". *Proceedings of the IEEE*, 89(12), 1808-1818, 2001.

24. Bove, R., and Ubertini, S., *Modeling solid oxide fuel cells: methods, procedures and techniques*. Springer Science & Business Media, 2008.

25. Huo, H., Ji, Y., Kuang, X., Liu, Y., and Wu, Y., "Dynamic modeling of SOFC based on support vector regression machine and improved particle swarm optimization", *Intelligent Control and Automation (WCICA),* pp. 1853-1858, IEEE, 2014.

26. Marzooghi, H., Raoofat, M., Dehghani, M., & Elahi, G. H., "Dynamic modeling of solid oxide fuel cell stack based on local linear model tree algorithm", *International journal of hydrogen energy*, 37(5), 4367-4376, 2012.

27. Das, T., and Snyder, S., "Adaptive control of a solid oxide fuel cell ultra-capacitor hybrid system", *IEEE Transactions on Control Systems Technology*, 21(2), 372-383, 2013.

28. Barelli, L., Cinti, G., Desideri, U., and Ottaviano, A., "SOFC thermal transients: modeling by application of experimental system identification techniques", *Fuel Cells*, 14(1), 107-122, 2014.

29. Pakalapati, S., Gerdes, K., Finklea, H., Gong, M., Liu, X., and Celik, I., "Micro scale dynamic modeling of LSM/YSZ composite cathodes", *Solid State Ionics*, 258, 45-60, 2014.

30. Yamamura, Y., Kawasaki S. and Sakai H. "Molecular dynamics analysis of ionic conduction mechanism in yttria-stabilized zirconia."*Solid State Ionics*, 181-189, 1999.

31. Perumal, T. P., Sridhar, V., Murthy, K. P. N., Easwarakumar, K. S., & Ramasamy, S., "Molecular dynamics simulations of oxygen ion diffusion in yttria-stabilized

32. Achenbach, E., "Three-dimensional and time-dependent simulation of a planar solid oxide fuel cell stack", *Journal of power sources*, 49(1), 333-348, 1994.

33. Padulles, J., Ault, G. W., and McDonald, J. R., "An integrated SOFC plant dynamic model for power systems simulation. *Journal of Power sources*, 86(1), 495-500, 2000.

34. Sedghisigarchi, K., and Feliachi, A., "Dynamic and transient analysis of power distribution systems with fuel Cells-part I: fuel-cell dynamic model", *IEEE transactions on energy conversion*, 19(2), 423-428, 2004.

35. Qi, Y., Huang, B., and Chuang, K. T., "Dynamic modeling of solid oxide fuel cell: The effect of diffusion and inherent impedance", *Journal of Power Sources*, 150, 32-47, 2005.

36. Campanari, S., and Iora, P., "Definition and sensitivity analysis of a finite volume SOFC model for a tubular cell geometry", *Journal of Power Sources*, 132(1), 113-126, 2004.

37. Wayland, H., *Differential equations applied in science and engineering*. No. 517.38 W39. 1957.

38. Welty, J. R., Wicks, C. E., Rorrer, G., and Wilson, R. E., *Fundamentals of momentum, heat, and mass transfer*. John Wiley & Sons, 2009.

39. Noren, D. A., and Hoffman, M. A., "Clarifying the Butler–Volmer equation and related approximations for calculating activation losses in solid oxide fuel cell models", *Journal of Power Sources*, 152, 175-181, 2005.

40. Chan, S. H., Khor, K. A., and Xia, Z. T., "A complete polarization model of a solid oxide fuel cell and its sensitivity to the change of cell component thickness", *Journal of Power Sources*, 93(1), 130-140., 2001.

41. Wagner, N., Schnurnberger, W., Müller, B., and Lang, M., “Electrochemical impedance spectra of solid-oxide fuel cells and polymer membrane fuel cells”., *Electrochimica Acta*, 43(24), 3785-3793, 1998.

42. Seborg, Dale E., *Process dynamics and control*. John Wiley & Sons, 2010.